

University of Wollongong

## Research Online

---

Faculty of Science, Medicine and Health -  
Papers: part A

Faculty of Science, Medicine and Health

---

1-1-2018

### Lajishankou Ophiolite Complex: Implications for Paleozoic Multiple Accretionary and Collisional Events in the South Qilian Belt

Changlei Fu

*Chinese Academy of Geological Sciences*

Zhen Yan

*Chinese Academy of Geological Sciences*

Zongqi Wang

*Chinese Academy of Geological Sciences*

Solomon Buckman

*University of Wollongong, solomon@uow.edu.au*

Jonathan C. Aitchison

*University of Queensland, jonathan.aitchison@sydney.edu.au*

*See next page for additional authors*

Follow this and additional works at: <https://ro.uow.edu.au/smhpapers>



Part of the [Medicine and Health Sciences Commons](#), and the [Social and Behavioral Sciences Commons](#)

---

#### Recommended Citation

Fu, Changlei; Yan, Zhen; Wang, Zongqi; Buckman, Solomon; Aitchison, Jonathan C.; Niu, Manlan; Cao, Bo; Guo, Xianqing; Li, Xiucan; Li, Yunshuai; and Li, Jiliang, "Lajishankou Ophiolite Complex: Implications for Paleozoic Multiple Accretionary and Collisional Events in the South Qilian Belt" (2018). *Faculty of Science, Medicine and Health - Papers: part A*. 5454.  
<https://ro.uow.edu.au/smhpapers/5454>

Research Online is the open access institutional repository for the University of Wollongong. For further information contact the UOW Library: [research-pubs@uow.edu.au](mailto:research-pubs@uow.edu.au)

---

# Lajishankou Ophiolite Complex: Implications for Paleozoic Multiple Accretionary and Collisional Events in the South Qilian Belt

## Abstract

The Lajishan ophiolite complex in the Qilian Orogen is one of several ophiolites situated between the Qaidam and North China blocks that record episodic closure of the Proto-Tethyan Ocean. Detailed field relations and geochemical and geochronological studies are critical to unraveling the tectonic processes responsible for an extensive period of intraoceanic subduction that produced juvenile ophiolite/island arc terranes, which were obducted onto continental margins during ocean closure. The Lajishankou ophiolite complex crops out along the northern margin of the South Qilian belt and was thrust over a Neoproterozoic-Ordovician passive margin sequence that was deposited upon the Proterozoic Central Qilian block. The mafic rocks in Lajishankou ophiolite complex are the most abundant slices and can be categorized into three distinct groups based on petrological, geochemical, and geochronological characteristics: massive island arc tholeiites, 509-Ma back-arc dolerite dykes, and 491-Ma pillow basaltic and dolerite slices that are of seamount origin in a back-arc basin. These results, together with spatial relationships, indicate that the Cambrian island arc rocks, ophiolite complex, and accretionary complex developed between 530 and 480 Ma as a single, intraoceanic arc-basin system as a result of south directed subduction of the Proto-Tethyan Ocean prior to Early Ordovician obduction of this system onto the Central Qilian block. Final continental amalgamation involved continental collision of the Central Qilian block with the Qaidam block during the Late Ordovician. This model solves the long-lasting discussion on the emplacement of the Lajishan ophiolite and contributes to an improved understanding of multiple accretionary and collisional processes in the Qilian Orogen.

## Disciplines

Medicine and Health Sciences | Social and Behavioral Sciences

## Publication Details

Fu, C., Yan, Z., Wang, Z., Buckman, S., Aitchison, J. C., Niu, M., Cao, B., Guo, X., Li, X., Li, Y. & Li, J. (2018). Lajishankou Ophiolite Complex: Implications for Paleozoic Multiple Accretionary and Collisional Events in the South Qilian Belt. *Tectonics*, 37 (5), 1321-1346.

## Authors

Changlei Fu, Zhen Yan, Zongqi Wang, Solomon Buckman, Jonathan C. Aitchison, Manlan Niu, Bo Cao, Xianqing Guo, Xiucai Li, Yunshuai Li, and Jiliang Li



## Tectonics

### RESEARCH ARTICLE

10.1029/2017TC004740

#### Key Points:

- The Lajishankou ophiolite complex consists of serpentinite, wehrlite, pyroxenite, gabbro, dolerite, pillow, and massive basalts
- The mafic rocks are geochemically similar to intraoceanic arc-basin remnants formed during southward subduction of the Proto-Tethyan Ocean
- Lajishan ophiolite-arc rocks were emplaced onto the Central Qilian block during arc-continent collision

#### Supporting Information:

- Supporting Information S1
- Table S1
- Table S2
- Table S3
- Table S4

#### Correspondence to:

Z. Yan,  
yanzhen@mail.iggcas.ac.cn

#### Citation:

Fu, C., Yan, Z., Wang, Z., Buckman, S., Aitchison, J. C., Niu, M., et al. (2018). Lajishankou ophiolite complex: Implications for Paleozoic multiple accretionary and collisional events in the South Qilian belt. *Tectonics*, 37, 1321–1346. <https://doi.org/10.1029/2017TC004740>





Received 2 AUG 2017

Accepted 29 MAR 2018

Accepted article online 19 APR 2018

Published online 10 MAY 2018

## Lajishankou Ophiolite Complex: Implications for Paleozoic Multiple Accretionary and Collisional Events in the South Qilian Belt

Changlei Fu<sup>1,2</sup> , Zhen Yan<sup>2</sup> , Zongqi Wang<sup>1</sup>, Solomon Buckman<sup>3</sup> , Jonathan C. Aitchison<sup>4</sup> , Manlan Niu<sup>5</sup>, Bo Cao<sup>2</sup>, Xianqing Guo<sup>1</sup>, Xiucui Li<sup>5</sup>, Yunshuai Li<sup>6</sup>, and Jiliang Li<sup>7</sup>

<sup>1</sup>MLR Key Laboratory of Metallogeny and Mineral Assessment, Institute of Mineral Resources, Chinese Academy of Geological Sciences, Beijing, China, <sup>2</sup>Institute of Geology, Chinese Academy of Geological Sciences, Beijing, China, <sup>3</sup>GeoQuEST Research Centre, School of Earth and Environmental Sciences, University of Wollongong, Wollongong, New South Wales, Australia, <sup>4</sup>School of Earth and Environmental Sciences, University of Queensland, Brisbane, Queensland, Australia, <sup>5</sup>Department of Resources and Environment, Hefei University of Technology, Hefei, China, <sup>6</sup>Institute of Surface-Earth System Science, Tianjin University, Tianjin, China, <sup>7</sup>Institute of Geology and Geophysics, Chinese Academy of Sciences, Beijing, China

**Abstract** The Lajishan ophiolite complex in the Qilian Orogen is one of several ophiolites situated between the Qaidam and North China blocks that record episodic closure of the Proto-Tethyan Ocean. Detailed field relations and geochemical and geochronological studies are critical to unraveling the tectonic processes responsible for an extensive period of intraoceanic subduction that produced juvenile ophiolite/island arc terranes, which were obducted onto continental margins during ocean closure. The Lajishankou ophiolite complex crops out along the northern margin of the South Qilian belt and was thrust over a Neoproterozoic-Ordovician passive margin sequence that was deposited upon the Proterozoic Central Qilian block. The mafic rocks in Lajishankou ophiolite complex are the most abundant slices and can be categorized into three distinct groups based on petrological, geochemical, and geochronological characteristics: massive island arc tholeiites, 509-Ma back-arc dolerite dykes, and 491-Ma pillow basaltic and dolerite slices that are of seamount origin in a back-arc basin. These results, together with spatial relationships, indicate that the Cambrian island arc rocks, ophiolite complex, and accretionary complex developed between 530 and 480 Ma as a single, intraoceanic arc-basin system as a result of south directed subduction of the Proto-Tethyan Ocean prior to Early Ordovician obduction of this system onto the Central Qilian block. Final continental amalgamation involved continental collision of the Central Qilian block with the Qaidam block during the Late Ordovician. This model solves the long-lasting discussion on the emplacement of the Lajishan ophiolite and contributes to an improved understanding of multiple accretionary and collisional processes in the Qilian Orogen.

### 1. Introduction

Many ophiolites represent relicts of ancient oceanic crust and upper mantle that have been tectonically emplaced onto continental margins during collision and/or subduction-accretion events (Coleman, 1977; Dewey & Bird, 1971; Dilek & Furnes, 2011; Nicolas, 1989; Moores, 1970). They commonly occur in association with suture zones as large well-preserved ophiolite bodies, such as the Coast Range ophiolite, which developed as elements of the upper plate above a subduction zone (Shervais, 1990; Wakabayashi, 2015, 2017a). Other smaller fragments of uppermost oceanic crust occur within accretionary complexes such as the Franciscan Complex. Such rocks are most likely to have been scrapped off the subducting oceanic plate and emplaced tectonically within the accretionary prism (Wakabayashi, 2017b, 2017c). Detailed studies of the Franciscan Complex and the Coast Range ophiolite and their analogues in ancient orogens like the Appalachians show that mafic rocks from the accretionary complex and upper plate ophiolites have distinctly different petrologic, structural, metamorphic, and geochemical characteristics (Hsü, 1968; Shervais, 1990; Zagorevski & van Staal, 2011; van Staal & Barr, 2012; Wakabayashi, 2015). Knowledge of these differences significantly improved our ability to discriminate between subduction-accretion and other geological processes. Field mapping and related studies of ophiolitic rocks, as well as discrimination between rocks from the upper plate or the accretionary complex, are essential to constraining the tectonic evolution of ancient subduction zones. This also provides insights into the multiple accretionary and collisional processes and

mechanisms of continental growth in complex orogenic systems such as central Asia (Buckman & Aitchison, 2004; Şengör et al., 1993; Xiao et al., 2015), Qinling (Dong & Santosh, 2016; Z. Wang et al., 2009), Qilian (Xia et al., 2016; Xiao et al., 2009), East Kunlun (Dong et al., 2018; Yu et al., 2017), and West Kunlun (Xiao et al., 2002, 2005) orogenic belts, where numerous Precambrian microcontinents formed and broke up during the Proterozoic and subsequently collided and were amalgamated during the Phanerozoic. This process of continental reassembly involved the periodic accretion and addition of numerous juvenile, oceanic terranes as well as the development of active continental margins (Aitchison & Buckman, 2012; Şengör et al., 1993; Xiao et al., 2015).

The Qilian orogenic belt (Figures 1a and 1b) formed in response to several discrete subduction events with different polarities as a result of closure of branches of the Proto-Tethyan Ocean and amalgamation of the Alxa and Qaidam blocks along the NE margin of Tibet (Song et al., 2014; Xia et al., 2016; Xiao et al., 2009; Yan et al., 2015; J. X. Zhang, Yu, & Mattinson, 2017). A distinctive structural feature of this complicated orogenic belt is a Proterozoic microcontinental fragment (Central Qilian block) that appears to separate the North Qilian and South Qilian suture zones (Figure 1b). Ophiolitic rocks are widely distributed within both the North and South Qilian belts (Fu & Yan, 2017; Qiu et al., 1997; Song et al., 2014; Xia et al., 2016; Xiao et al., 2009, and references therein).

In the South Qilian belt, basalt, gabbro, ultramafic cumulate rocks, chert, limestone, and rare mantle peridotites of Cambrian age are exposed discontinuously and display the characteristic features of a dismembered ophiolite (Fu & Yan, 2017; Yan et al., 2015). The Lajishan ophiolite belt is the largest single zone within the belt with a length of 200 km and a width of 10–30 km. Therefore, its origin and tectonic setting are of importance for understanding the tectonic evolution of the orogen. Due to structural complexity and a lack of systematic field and petrologic studies, exact lithological assemblages, timing of emplacement, and tectonic settings remain unclear making regional correlations difficult. For instance, volcano-sedimentary units in Lajishan are assigned a Cambrian age based on trilobite faunas from limestones (Lin et al., 2015, and references therein). However, isotopic ages for critical lithologies and sedimentary provenance study are lacking and whether the limestones are autochthonous or they represent older allochthonous blocks slumped into younger sequences remains to be determined. Geochemical data indicate that Cambrian-aged basalts are mainly transitional between mid-ocean ridge basalt (MORB) and within plate basalt (Hou et al., 2005; Qiu et al., 1997) or ocean island basalt (OIB) (Hou et al., 2005; Y. Zhang, Song, et al., 2017) with some exhibiting island arc affinity (Qiu et al., 1997). Several models such as a continental rift (Qiu et al., 1997), back-arc basin (Gao, 2000), multistage uplifted structure window (E. Wang et al., 2000), and a subduction-accretionary complex (Xiao et al., 2009; Yan et al., 2015, and references therein) have been proposed to explain the tectonic evolution of the South Qilian belt without any consistent consensus being reached. A key problem within such a fragmented orogenic zone is that some “ophiolitic” rocks may represent small, disrupted bodies within subduction complexes that were accreted from the downgoing plate. Alternatively, they may simply represent relicts of suprasubduction zone (SSZ) ophiolites. Geological mapping, geochronology, and geochemistry are critical to regional-scale correlation between multiple ophiolitic rocks.

In this paper, we describe field occurrences of the Lajishan ophiolite and accretionary complex in the Liutai, Xigou, and Lajishankou areas, based on observations made during our geological mapping program. Zircon U-Pb ages, mineralogy, petrology, geochemistry, and Sr-Nd data from mafic rocks of the Lajishankou ophiolite complex are also reported. Finally, we discuss the geodynamic setting and likely mantle source of these mafic rocks in order to determine the tectonic processes responsible for generation of rocks occurring within the Lajishan ophiolite and accretionary complex.

## 2. Geological Setting

The ~300-km-wide, ~1,200-km-long Qilian Orogen belt trends NW-SE along the NE margin of the Tibetan Plateau and is also the northernmost orogenic collage of the Tethyan domain. It is separated from the Tarim block to the west by the Altyn Tagh Fault, while a Cenozoic basin runs along the boundary with the Qinling-Dabie orogen to the SE (Figure 1a). It is subdivided into three fault-bounded belts. From north to south these are (1) North Qilian, (2) Central Qilian, and (3) South Qilian belts (Figure 1b; Feng et al., 2002). The North Qilian belt is ~1,200-km-long, ~100-km-wide and lies between Alxa block to the north and the Qilian block to the south (Figure 1b). This belt is considered to be the most extensively studied part and is



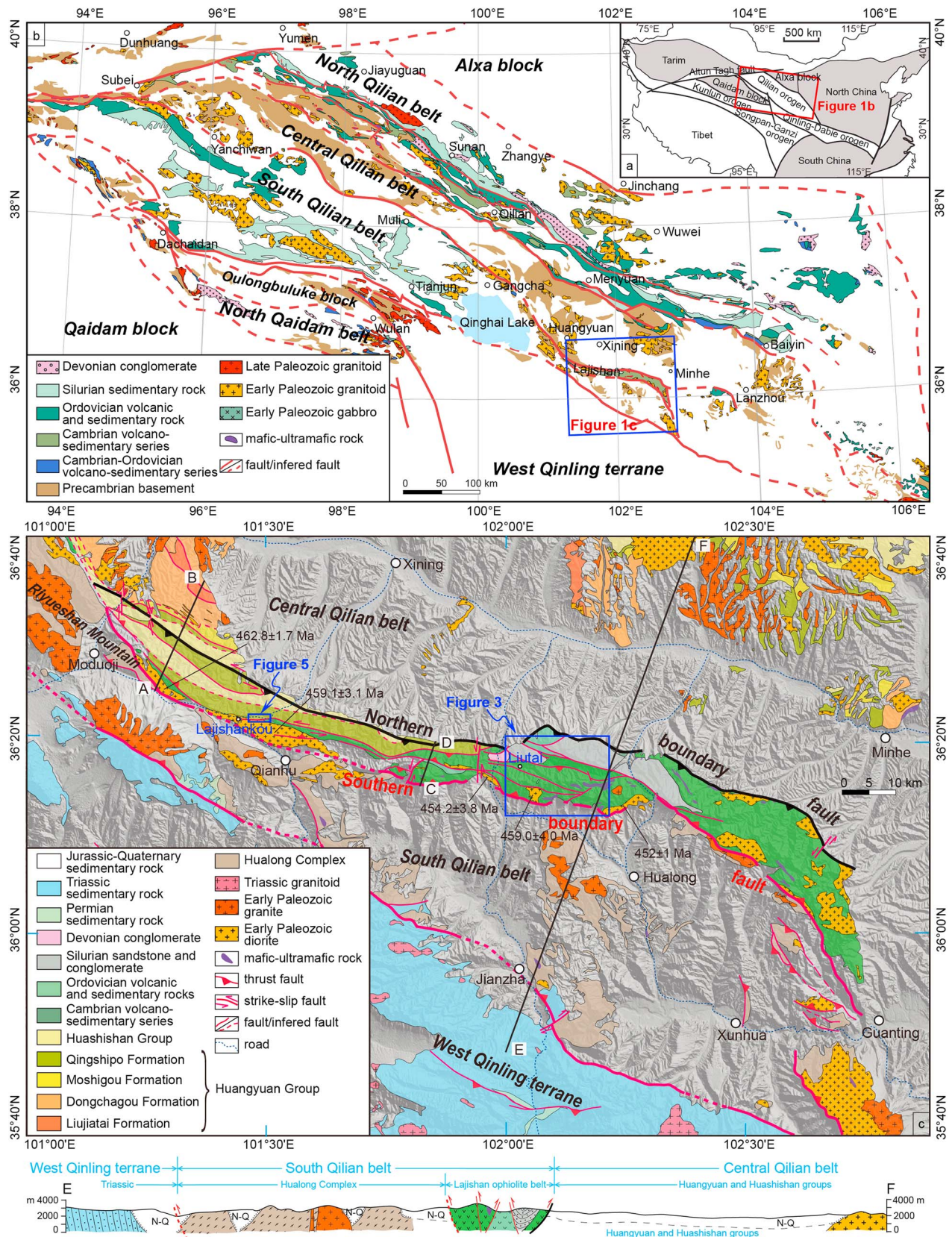


**Figure 1.** (a) Tectonic framework of China and location of the Qilian Orogen. (b) Simplified geological map of the Qilian Orogen and location of the study area. (c) Geological map and cross section of the Lajishan and adjacent areas. For additional details of part of legend, see Figure 2.



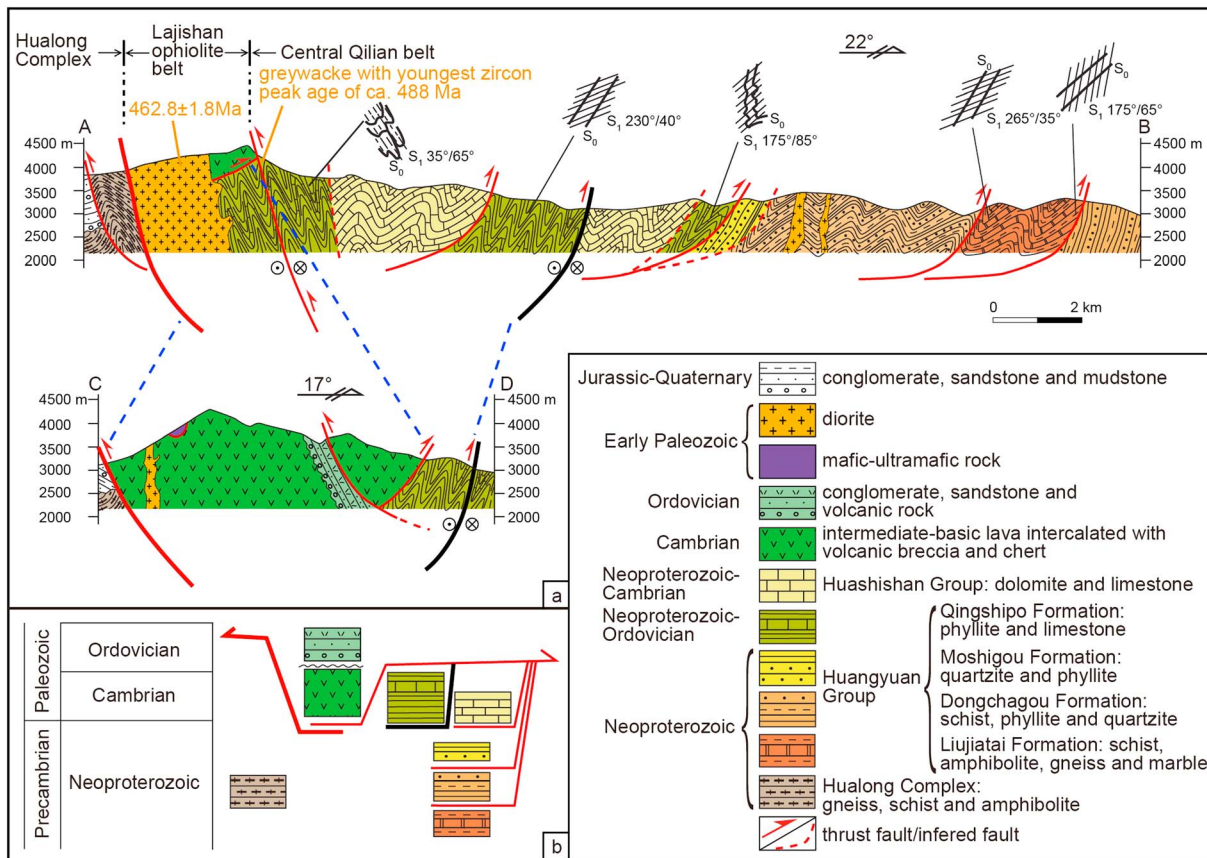


**Figure 2.** (a) Geological cross sections across the Lajishan ophiolite complex showing the structural relationships between the different stratigraphic units (locations see Figure 1c; modified from Guo & Li, 1999). Youngest detrital zircon peak age for greywacke of the Qingshipo Formation and age of granitoid without references are from unpublished data of Zhen Yan. (b) Schematic diagram illustrating the relationships between tectonostratigraphic units in the Lajishan ophiolite belt and the South Qilian and Central Qilian blocks.

typical of a Marianan-type intraoceanic subduction system in that it includes elements recognizable as parts of an accretionary prism, ophiolite, seamount, island arc, and back-arc/fore-arc basins (Xiao et al., 2009; Yan et al., 2010, and references therein).

The Central Qilian belt is approximately 1,000-km long and 50- to 80-km wide and separated from the North Qilian and South Qilian by SW verging thrust faults, respectively. It is dominated by Precambrian lower greenschist- to amphibolite-facies metamorphic rocks (Wan et al., 2003, and references therein) intruded by Paleozoic S- and I-type granitoids (Huang et al., 2015; Xiao et al., 2009; Yang et al., 2016). In the central part of Central Qilian belt, the 240-km-long and 80-km-wide zone of Precambrian metamorphic rocks near Huangyuan area were originally defined as the Neoproterozoic Huangyuan and Huashishan groups respectively by the Bureau of Geology and Mineral Resources of Qinghai Province (BGMQRQ, 1964). Together with the Neoproterozoic Hualong Complex in the South Qilian belt, they are interpreted as microcontinental blocks that separated from the South China plate in the late Neoproterozoic (Guo & Li, 1999; Wan et al., 2003; Yan et al., 2015).

The Huangyuan Group is composed of schist, amphibolite, gneiss, marble, quartzite, and phyllite, which was subdivided into four lithostratigraphic units, in ascending order: Liujiatai, Dongchagou, Moshigou, and Qingshipo formations based on lithology and geologic ages (Figures 1c and 2; BGMQRQ, 1964). The Liujiatai, Dongchagou, Moshigou, and Qingshipo formations are repeated by folding or faulting and have thicknesses of ~1,100, 750–1,700, 540–670, and 420–2,400 m, respectively (BGMQRQ, 1964). In 1991, the Bureau of Geology and Mineral Resources of Qinghai Province separated the Moshigou and Qingshipo formations from the Huangyuan Group and redefined them as the Huangzhong Group according to their different rock assemblages and metamorphic grades. However, Guo et al. (2000) suggested that they share

similar protoliths and referred them as the Huangyuan Group. Lithological assemblages and abundant quartzites within the Liujiatai, Dongchagou, and Moshigou formations indicate deposition in a littoral, neritic environment (Guo et al., 1999). On the other hand, greywacke, siltstone, and mudstone in the Qingshipo Formation show features typical of turbidites deposited in deepwater environment of a passive continental margin (Guo et al., 1999; Guo & Li, 1999). The formation age of the Huangyuan Group is traditionally assigned to the Paleoproterozoic, based on earlier single-grain zircon U-Pb and whole rock Rb-Sr and Sm-Nd isotope age determinations (BGMRQP, 1991). More recent zircon U-Pb age determinations from granitoids, granitic gneisses, and metavolcanic rocks in the Huangyuan Group range from circa 930 to 750 Ma, indicating that much of the Huangyuan Group formed during Neoproterozoic time (Guo et al., 2000; Wan et al., 2003). We recently obtained a youngest detrital zircon age peak of circa 488 Ma from greywacke of the Qingshipo Formation (Figure 2). This result, together with Ordovician ages for diorites, which intruded into the Qingshipo Formation, further suggests that the upper age limit for the Qingshipo Formation is Ordovician.

The Huashishan Group mainly consists of weakly metamorphosed dolomite and limestone, with minor phyllite and chert interlayers attaining a thickness of 500–1,400 m (BGMRQP, 1964). Carbonates in the Huashishan Group are characterized by oolites, breccias, and stromatolites (Guo et al., 1999; Guo & Li, 1999), indicating a high-energy littoral and neritic environment. This unit is assigned to Mesoproterozoic Jixian period based on reports of algal fossils (BGMRQP, 1991). However, the angular unconformity between the Huangyuan Group and the Huashishan Group and fragments of *Chanceloria* sp., trilobites, ostracoda, pelecypod, and crinoid stem fragments in the Huashishan Group suggest that it may represent a stable sedimentary cover of Sinian to Cambrian age deposited on passive continental margin rather than the Precambrian basement of Central Qilian block (Guo et al., 1999; Guo & Li, 1999, and references therein).

The South Qilian belt is approximately 800-km long and 50- to 120-km wide and is dominated by the Neoproterozoic Hualong complex, Cambrian-Ordovician volcano-sedimentary and ultramafic rocks, and minor Silurian-Devonian siliciclastic rocks (Figures 1b, 1c, and 2) (BGMRQP, 1964, 1991). The Hualong Complex is around 140-km long and 5- to 40-km wide and is mainly composed of felsic magmatic rocks, cherts, turbiditic sediments and mafic rocks metamorphosed to gneisses, schists, and amphibolites (Figures 1c and 2; Fu et al., 2018; Yan et al., 2015) that are intruded by early Paleozoic granitoids and mafic rocks (Yan et al., 2015). It has been interpreted as an arc-accretionary complex formed by the subduction-accretion of oceanic plate material during Ordovician times (Xiao et al., 2009; Yan et al., 2015, and references therein). Cambrian volcano-sedimentary rocks consist of pillow basalt, andesite, rhyolite, volcanic breccias, chert, and lenses of limestone, while the Ordovician rocks mainly consists of andesite, rhyolite, andesitic and rhyolitic breccias, and volcanoclastic rocks (Figures 1c, 2, and 3). They are unconformably overlain by Silurian to Devonian nonmarine deposits, mainly comprising conglomerate, pebbly sandstone, and siltstone with trough cross-bedding and imbricated pebbles. Regional mapping demonstrates that ultramafic rocks include slices of peridotite, serpentinite with little or no olivine and pyroxene relics, and pyroxenite of different sizes up to 3 km by 1.5 km in map dimension that crop out discontinuously at Yanchiwan, Muli, and Lajishan along the northern margin of the South Qilian belt (Figure 1c). Together with ultramafic rocks at Lajishan, Cambrian gabbro, plagiogranite, mafic rocks, chert, and limestone constitute the Lajishan ophiolite complex (Figure 3; Fu & Yan, 2017; Yan et al., 2015).

### 3. Lajishan Ophiolite and Accretionary Complex

The Lajishan ophiolite complex is 200-km long and 10- to 30-km wide and located between the Central and South Qilian belts (Figures 1b and 1c). It extends from Riyueshan Mountain in the west in an easterly direction to Guanting village in Minhe County. It is fault-bounded and juxtaposed against the Proterozoic Huangyuan Group to the north and the Neoproterozoic Hualong Complex to the south (BGMRQP, 1964; Yan et al., 2015).

Structural and geological cross sections across the Lajishan ophiolite complex indicate that the structures along the southern margin of the Central Qilian belt are dominated by NNW-SSE trending thrust faults, tight folds, and foliations (Figures 1c and 2a; Guo & Li, 1999). Early stage deformation is characterized by compressive deformation recorded by NE verging thrust faults, folds, and SW dipping foliations resulting in NE direct thrusting of Cambrian volcano-sedimentary and ultramafic rocks onto the Qingshipo Formation (Figure 2). In the southern parts of the cross sections, the Lajishan Cambrian volcano-sedimentary series and Ordovician



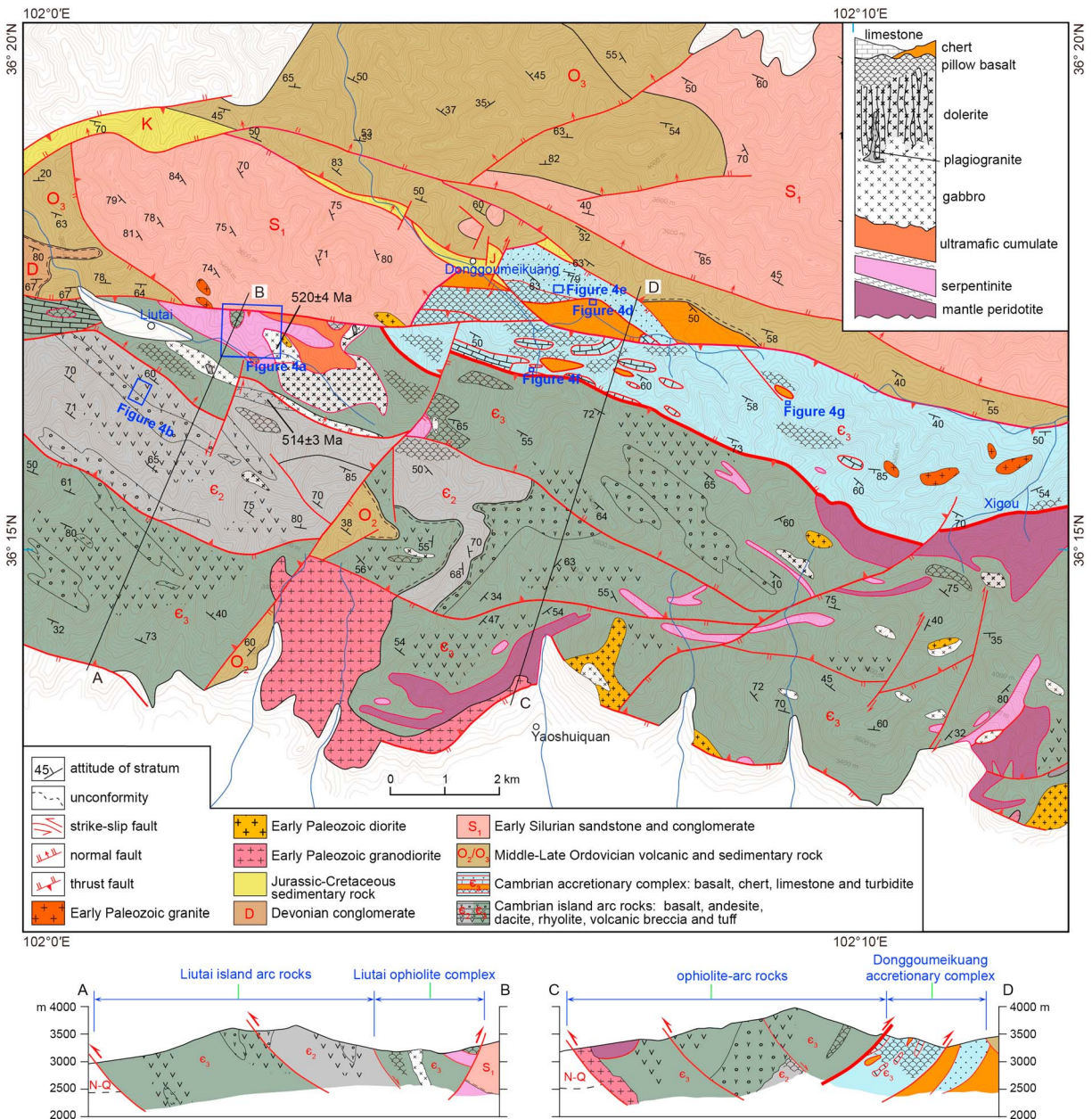


**Figure 3.** Geological map and cross sections of the central part of Lajishan and inferred composite crustal column through the Lajishan ophiolite complex. The geological map is based on our geological mapping results in the Liutai, Donggoumeikuang, and Xigou areas as well as published results from BGMQRQ (1977).

volcanic and sedimentary rocks have been thrust onto the Neoproterozoic Hualong Complex. SW verging thrust faults which crosscut the NE verging faults and Ordovician diorites (Figure 2) developed in the Lajishan area and the South Qilian block during late-stage deformation.

The Lajishan ophiolite complex is varied and different lithological assemblages crop out at each location. At Xigou, it consists of mantle peridotite, serpentinite, gabbro, dolerite, and basalt (Figure 3), whereas at Liutai it is mainly composed of serpentinite, pyroxenite, gabbro, plagiogranite, dolerite, and basalt (Figures 1c, 3, and 4a; Fu & Yan, 2017). To the south, the ophiolite complex is in fault contact with Middle Cambrian volcanic rocks including basalt, andesite, dacite, rhyolite, and volcanic breccias with island arc geochemical affinity (Figures 3, 4b, and 4c; Fu & Yan, 2017). To the north, the ophiolite-arc rocks are tectonically separated from the Cambrian accretionary complex by a NE verging thrust fault (Figure 3). The Donggoumeikuang accretionary complex is dominated by pillow basalts (Figure 3) with MORB and OIB affinities (Fu & Yan, 2017) and also



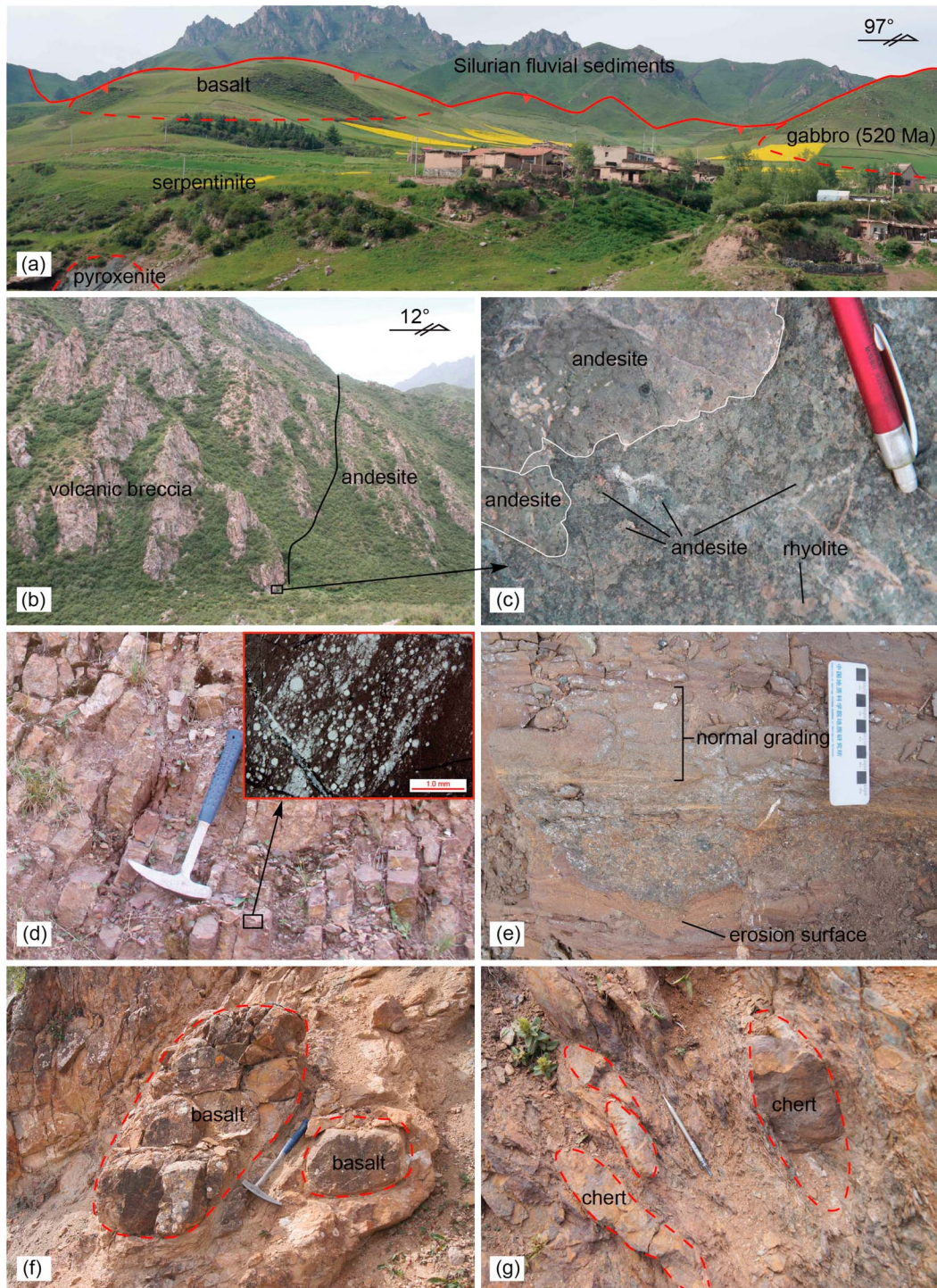


**Figure 4.** Photographs of field occurrences of ophiolite complex (a), island arc rocks (b, c), and accretionary complex (d–g) from the Liutai area (for locations see Figure 3). (a) Ophiolite complex at Liutai (foreground) consisting of serpentinite, pyroxenite, gabbro, and dolerite in fault contact with Silurian conglomerate and sandstone ( $36^{\circ}16'43.70''\text{N}$ ,  $102^{\circ}2'48.74''\text{E}$ ). (b, c) Volcanic breccia with clasts of andesite and rhyolite deposited upon andesite ( $36^{\circ}16'4.18''\text{N}$ ,  $102^{\circ}2'3.75''\text{E}$ ). (d) Radiolarian chert in outcrop and under plane polarized light ( $36^{\circ}17'20.53''\text{N}$ ,  $102^{\circ}6'46.65''\text{E}$ ). (e) Erosional surface and normal grading in turbidite ( $36^{\circ}17'33.35''\text{N}$ ,  $102^{\circ}6'31.23''\text{E}$ ). (f) Basalt blocks embedded in siliciclastic matrix ( $36^{\circ}16'35.21''\text{N}$ ,  $102^{\circ}6'8.83''\text{E}$ ). (g) Chert blocks embedded in siliciclastic matrix ( $36^{\circ}16'25.26''\text{N}$ ,  $102^{\circ}9'5.87''\text{E}$ ).



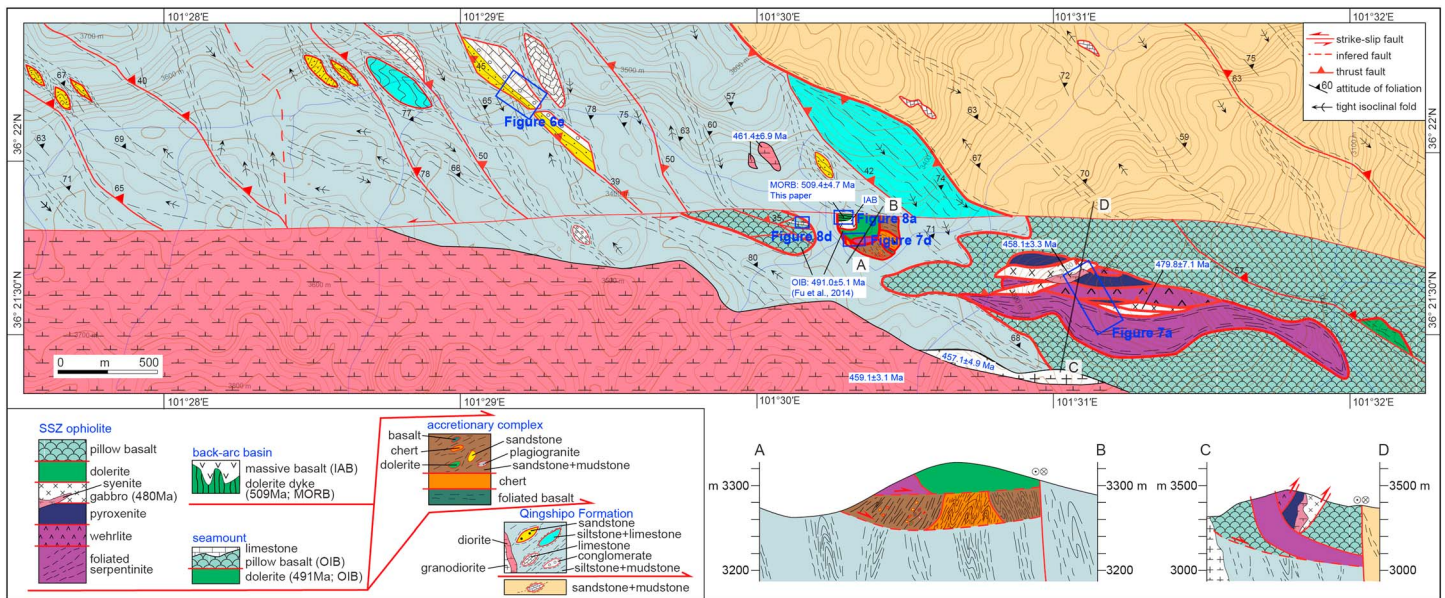


**Figure 5.** Geological map and cross sections of the Lajishankou ophiolite complex. In order to show the compositions of Lajishankou ophiolite and accretionary complex and structural relationships between the different lithotectonic units, the horizontal and vertical scales of section A-B are enlarged. Ages of granitoids and gabbro without references are from unpublished data of Zhen Yan. IAB = island arc basalt; MORB = mid-ocean ridge basalt; OIB = ocean island basalt.

includes black and red radiolarian chert (Figure 4d), limestone, and turbiditic sandstone (Figures 3 and 4e). The basalts and associated sedimentary rocks are repeated by NE verging thrusts in duplexes (Figure 3). Locally, the basalt or chert is highly disrupted and enveloped within a siliciclastic matrix (Figures 4f and 4g).

Our geological mapping and petrological investigations suggest that the Lajishankou ophiolite complex consists of numerous different thrust slices, which were emplaced onto the Qingshipo Formation (Figures 2 and 5). At Lajishankou, the Qingshipo Formation is mainly composed of fine-grained gray sandstone, silty mudstone, and muddy limestone (Figures 5, 6a–6d, and 7e). Basal erosion, graded bedding (Figure 6a), ripple, and parallel lamination indicate turbiditic origins. These sedimentary rocks are strongly deformed and characterized by compressive and shear deformation recorded by imbricate thrusts (Figure 5), isoclinal folds (Figures 6b and 6c), foliations (Figures 6c and 6d), and boudinage (Figure 6d). Sandstones mainly consist of quartz and minor plagioclase and lack any fragments of ophiolitic provenance (Figure 6b). The quartz-arenite, conglomerate, limestone, and thin muddy limestone assemblage is lenticular and in fault contact with turbidites composed of shale and muddy siltstone (Figure 6e). However, oblique beddings (Figure 6f), planar cross bedding (Figure 6g), and pebble imbrication (Figure 6h) within these blocks indicate that they were deposited in a tidal environment. Detrital zircon U-Pb age-dating results demonstrate that the quartz-arenites were derived from 1183- to 2073- and 2400- to 3266-Ma sources, which is distinctly different from turbiditic siltstone with a mixed source of 906 and 488 Ma. This suggests that these lenticular assemblages should be of exotic origin and older than the turbidites.

The Lajishankou ophiolite complex includes ultramafic rocks, cumulate gabbro, dolerite, and basalt that occur in a series of elongate fault-bounded slices (Figures 5 and 7a). Ultramafic lithologies include serpentinite, wehrlite, and pyroxenite representing a former mantle-crust transition zone that once lay between mantle peridotites and gabbros (Figures 7a and 7b) (Boudier & Nicolas, 1995; Jouselin & Nicolas, 2000). Cumulate layering is preserved in gray to dark green fine to medium-grained gabbro that is intruded by Ordovician syenite (Figures 5 and 7a). Serpentinites are strongly deformed and sheared without olivine and pyroxene relics. Several slices of wehrlite, pyroxenite, and gabbro form nodular or lenticular bodies striking WNW (Figure 7a).

Dolerites and basalts are the predominant slices of the Lajishankou ophiolite complex. Based on field occurrences and petrography, dolerites are classified into two types: (1) dolerite dykes and (2) dolerite slices. The dykes intrude gray massive basalts (Figures 8a and 8b). Subvertical calcite veins are common within massive basalts and dolerite dykes. The ~100-m-wide dolerite slices are in fault contact with serpentinite and



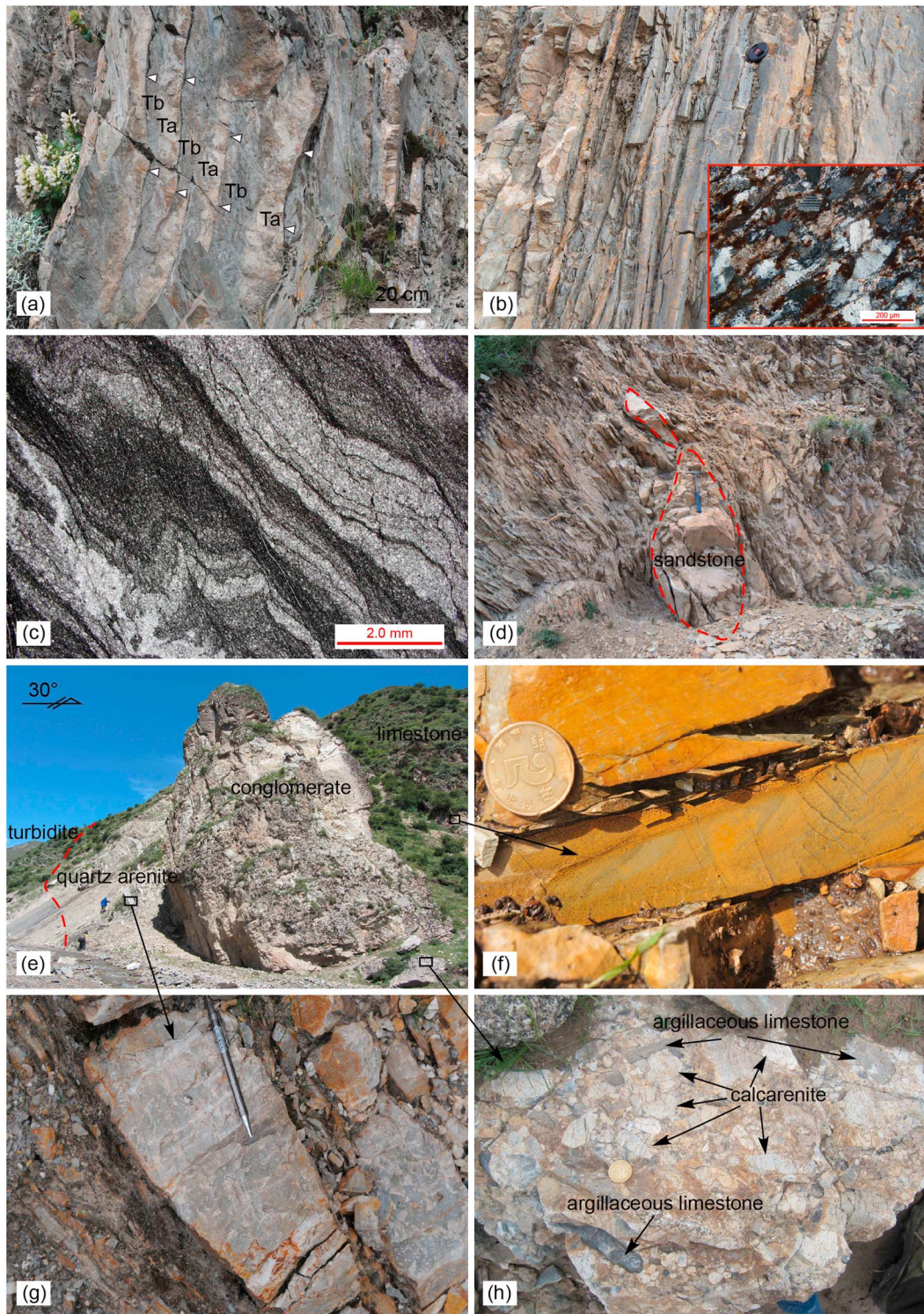


**Figure 6.** Photographs of field occurrences and photomicrographs of sedimentary rocks from the Qingshipo Formation at Lajishankou. (a) Incomplete Bouma sequence with distinct basal erosion (arrowheads), normal grading (Ta), and parallel lamination (Tb; 36°22′14.15″N, 101°28′26.80″E). (b) Tight isoclinal folds preserved in sandstone (36°22′4.15″N, 101°28′6.42″E). The sandstone is composed of quartz and minor plagioclase. (c) Folded mudstone under plane polarized light. (d) Sandstone boudins within a foliated siltstone matrix (36°22′11.84″N, 101°28′38.23″E). (e) Exotic sedimentary rocks consisting of quartz sandstone, conglomerate, and limestone in fault contact with turbidites (36°22′8.74″N, 101°29′13.08″E). (f) Limestone with oblique bedding. (g) Gray, medium quartz arenite with cross bedding. (h) Conglomerate with subrounded pebbles of argillaceous limestone, and calcarenite.





**Figure 7.** Photographs of field occurrences and photomicrographs of representative rocks from the Lajishankou ophiolite and accretionary complex. (a) Relationships between serpentinite, wehrlite, pyroxenite, cumulate gabbro, and syenite ( $36^{\circ}21'34.78''\text{N}$ ,  $101^{\circ}30'51.26''\text{E}$ ). (b) Wehrlite intrusive into pyroxenite ( $36^{\circ}21'40.30''\text{N}$ ,  $101^{\circ}31'9.59''\text{E}$ ). (c) Microtexture of mélangé with sandstone blocks (S) in a muddy (M) matrix. (d) Serpentinite and dolerite resting on accretionary complex consisting of basalt, chert, and mélangé ( $36^{\circ}21'44.97''\text{N}$ ,  $101^{\circ}30'23.51''\text{E}$ ). (e) Mélangé containing blocks of plagiogranite, dolerite, basalt, chert, and sandstone in a muddy matrix. (f) Foliated basalt composed of primary plagioclase (Pl) and secondary actinolite (Act). (g) Foliated radiolarian chert.

tectonically overlie the accretionary complex (Figures 5 and 7d). Other basalts commonly show pillow structures (Figure 8c) in outcrop and minor limestone interlayers (Figure 8d) also occur. The pillows vary between 0.25 and 1 m in diameter.



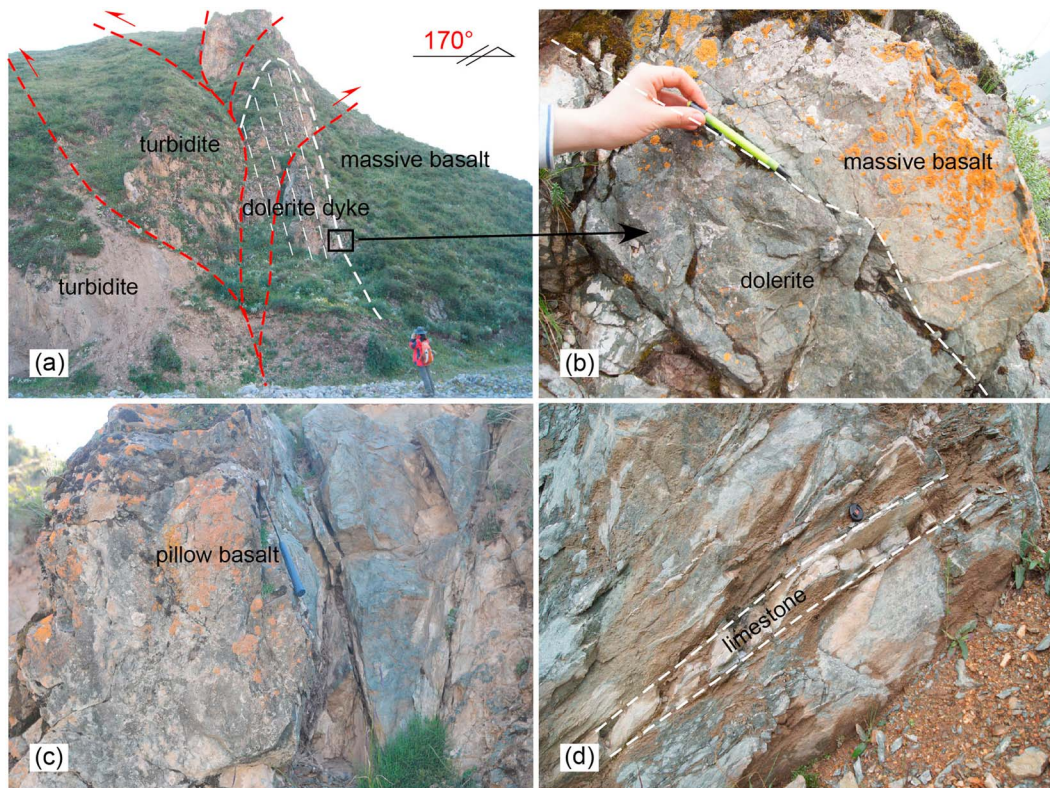


**Figure 8.** (a) Relationships between dolerite dykes, massive basalts, and turbidites ( $36^{\circ}21'48.63''\text{N}$ ,  $101^{\circ}30'11.28''\text{E}$ ). (b) Dolerite intrusive into basalt. (c) Pillow basalts ( $36^{\circ}21'47.76''\text{N}$ ,  $101^{\circ}30'43.27''\text{E}$ ). (d) Pillow basalt with intercalation of limestone ( $36^{\circ}21'45.38''\text{N}$ ,  $101^{\circ}30'8.56''\text{E}$ ).

The accretionary complex lies structurally beneath the ophiolite complex and is composed mainly of basalt, radiolarian chert, sandstone, mudstone, and mélange (Figures 5 and 7d–7g). Together, these rocks represent highly deformed tectonic slices bounded by faults and zones of mélange. The basalt and radiolarian chert are strongly sheared (Figures 7f and 7g). The foliated basalts mainly consist of primary plagioclase, secondary actinolite, and minor epidote commensurate with greenschist facies metamorphism (Figure 7f). About 10% of this accretionary complex consists of a mud-matrix mélange composed of various exotic blocks, including plagiogranite, dolerite, basalt, chert, and sandstone, within a highly sheared muddy matrix (Figures 7c and 7e).

These structural and petrological investigations suggest that the Lajishan ophiolite complex structurally overlies the accretionary complex, which crops out discontinuously along the northern margin of the Lajishan ophiolite. Abundant felsic-intermediate rocks of arc origin distributed near the ophiolite complex also suggest that the arc and ophiolite rocks are elements of the same intraoceanic subduction complex that was thrust over the passive continental margin of the Central Qilian block.

#### 4. Petrography of Mafic Rocks in the Lajishankou Ophiolite Complex

Massive basalts exhibit intergranular textures characterized by subhedral plagioclase with a grain size of 0.02–0.15 mm (Figure 9a) and subhedral clinopyroxene with a grain size of 0.02–0.1 mm. Some contain secondary epidote, chlorite, quartz, and minor actinolite (Figure 9b). These secondary minerals may have formed during hydrothermal activity associated with the intrusion of the dolerite dykes (Figure 8b).

Dolerite dykes display ophitic textures and consist of 55% plagioclase, 40% clinopyroxene, minor chlorite, pyrite, and calcite (Figure 9c). Plagioclase laths are euhedral but severely altered to kaolinite and/or sericite (Figure 9c). Clinopyroxenes are interstitial to plagioclases and their borders are transformed into chlorite. Dolerite slices exhibit gabbroic-diabasic textures, with an assemblage of 50% plagioclase, 45%



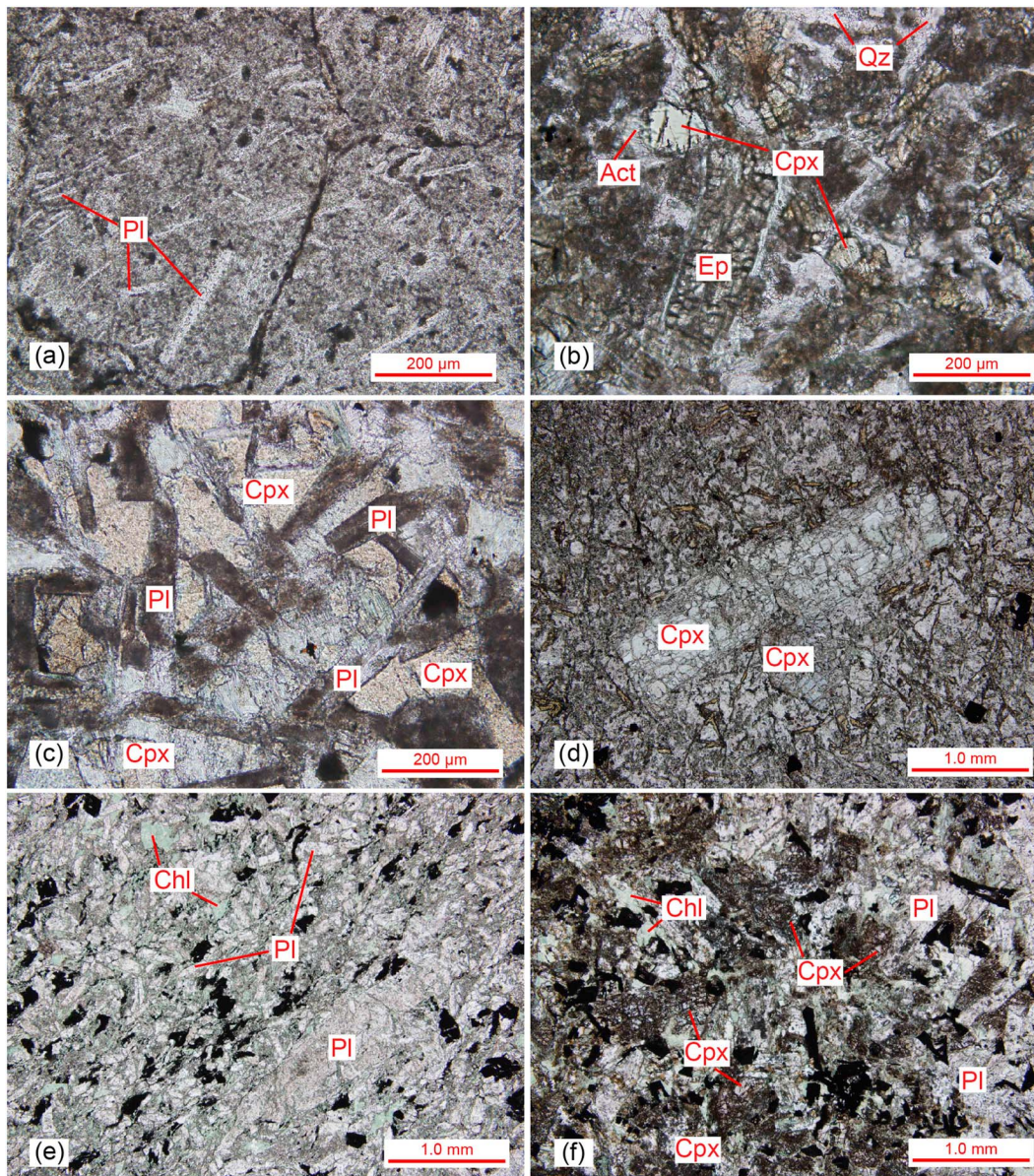


**Figure 9.** (a, b) Massive basalt (14LJ2) consisting of plagioclase, clinopyroxene, epidote, quartz, and minor actinolite. (c) Dolerite dyke (11LJS76) with ophitic texture. (d, e) Pillow basalt (12LJ74, 11LJS57) with a porphyritic texture. (f) Dolerite slice (11LJS85) with a gabbroic-diabasic texture. Act = actinolite; Chl = chlorite; Cpx = clinopyroxene; Ep = epidote; Pl = plagioclase; Qz = quartz.

clinopyroxene, chlorite, and Fe-Ti oxides (Figure 9f). Plagioclases are relatively subhedral and vary from 0.2 to 0.5 mm in size. The clinopyroxenes are subhedral and partly metamorphosed to chlorite.

Pillow basalts exhibit porphyritic textures with phenocrysts of clinopyroxene and minor plagioclase (Figures 9d and 9e). Clinopyroxene phenocrysts are 1–2 mm in size and display crossed twinning. Minor plagioclase phenocrysts are 0.5–2 mm in size and display polysynthetic twinning (Figure 9e). The groundmass is composed of plagioclase microlites, granular clinopyroxene, chlorite, and opaque (Fe-Ti oxide) minerals (Figures 9d and 9e). Plagioclases in the groundmass are subhedral and range from 0.1 to 0.2 mm in size. Many clinopyroxenes are partially to completely replaced by chlorite and opaque minerals (Figure 9e).

These petrographic and structural characteristics indicate that the less deformed mafic rocks from the Lajishankou ophiolite complex are distinct from those within the underlying strongly deformed



accretionary complex, which have undergone high-grade (greenschist facies) burial metamorphism. Therefore, the Lajishankou ophiolite complex may be part of the upper plate above a subduction zone.

## 5. Analytical Methods

### 5.1. Mineral Chemistry

Pyroxenes from mafic rocks were analyzed at the Institute of Mineral Resources, Chinese Academy of Geological Sciences, using a JEOL JXA-8800R electron probe with a 20 kV accelerating voltage, 20-nA beam current and a 5- $\mu\text{m}$  beam.

### 5.2. Major and Trace Elements

Twenty-two representative and relatively fresh samples were collected for geochemical analysis. Samples were cleaned and all weathered and veined surfaces were removed. Each sample was powdered using an agate mill, and fused glass beads were prepared for major element analysis utilizing a Phillips PW 4400 X-ray fluorescence spectrometer with a rhodium X-ray source. FeO content was determined by digestion with HF and H<sub>2</sub>SO<sub>4</sub> and titration with standard potassium dichromate solution, using the diphenylamine sulphate indicator. Loss on ignition was measured by weighing before and after 1 hr in a furnace at 1000 °C. All major and trace elements were analyzed at the National Research Center, Chinese Academy of Geological Sciences, Beijing. International standards GSR1, GSR2, and GSR3 were used to monitor analytical quality control. Detection limits for major elements were < 0.01% (except for TiO<sub>2</sub> and MnO, which had detection limits <0.001%). Detection limits for minor and trace elements were 1–0.05 ppm. Based on the analyses of international reference materials, the analytical precision for all major oxides by X-ray fluorescence is estimated to be better than 1%. Trace element concentrations were determined by inductively coupled plasma mass spectrometry using a VG Elemental PQII Plus system. All measurements of the trace elements were corrected for instrumental drift using the peak intensities of 115 In and 185 Re internal monitors. The results of standard analyses are consistent with their reference values within the published error ranges, respectively, with the differences for trace elements, including rare earth element (REE), within 5–10%. Details of trace element analytical procedures have been described by Liang et al. (2000).

### 5.3. Zircon U-Pb Ages

Fifty zircon grains from a 20-kg dolerite dyke sample (13LJ) and 250 zircon grains from a 20-kg dolerite slice (11LJS81) were extracted using standard heavy liquid and magnetic techniques. They were handpicked under a binocular microscope and mounted in epoxy resin. The sample mount was polished to expose the center of the zircon grains and then gold coated. Reflected and transmitted light photographs and cathodoluminescence (CL) images were acquired to reveal internal structures and to target specific areas therein. The CL images were obtained by scanning electron microscopy using a FEI PHILIPS XL 30 SFEG instrument with a 2-min scanning time at conditions of 15 kV and 120 nA. U-Th-Pb zircon dating was performed on the SHRIMP II at Beijing SHRIMP Center, Institute of Geology, Chinese Academy of Geological Sciences. Operation and data processing follow Williams (1998). Standard M257 (561 Ma) was measured to calibrate U, Th, and Pb contents, and the standard zircon TEM (417 Ma) was used for element fractionation correction. All the data were assessed using the Squid and Isoplot programs. Common Pb was corrected using the measured <sup>204</sup>Pb. Ages were calculated using International Union of Geological Sciences recommended coefficients. The errors given in the data tables for individual analyses are quoted at the 1 $\sigma$  level, whereas the errors for weighted mean ages are at the 2 $\sigma$  confidence level. Discussion of age data is based on <sup>206</sup>Pb/<sup>238</sup>U ages for zircons younger than 1000 Ma and <sup>207</sup>Pb/<sup>206</sup>Pb ages for those older than 1000 Ma.

### 5.4. Sr-Nd Isotopes

Eight samples were selected for Sm-Nd isotopic analysis and measured at Institute of Geology and Geophysics, Chinese Academy of Sciences. The Rb-Sr and Sm-Nd isotopic analysis followed procedures similar to those described by Li et al. (2011). Whole rock powders for Sr and Nd isotopic analyses were dissolved in Savillex Teflon screw top capsule after being spiked with the mixed <sup>87</sup>Rb-<sup>84</sup>Sr and <sup>149</sup>Sm-<sup>150</sup>Nd tracers prior to HF + HNO<sub>3</sub> + HClO<sub>4</sub> dissolution. Rb, Sr, Sm, and Nd were separated using the classical two-step ion exchange chromatographic method and measured using a Finnigan MAT262 multicollector thermal ionization mass spectrometer at Institute of Geology and Geophysics, Chinese Academy of Sciences. The whole procedure blank was lower than 300 pg for Rb-Sr and 100 pg for Sm-Nd. The isotopic ratios were corrected for mass

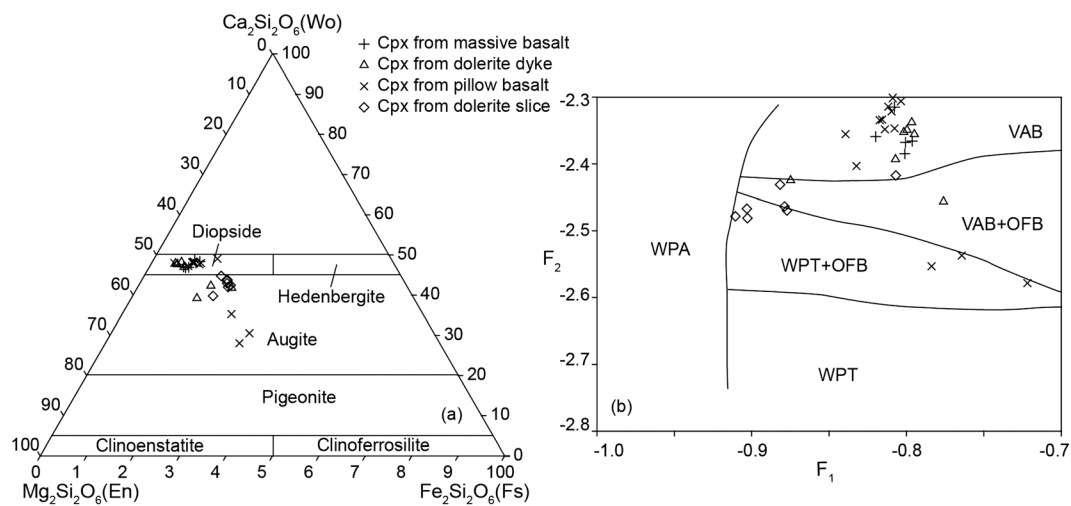


**Figure 10.** (a) Compositions of clinopyroxenes (after Morimoto, 1988) and (b) discriminant diagram (after Nisbet & Pearce, 1977) for clinopyroxenes from mafic rocks of the Lajishankou ophiolite complex. OFB = ocean floor basalt; VAB = volcanic arc basalt; WPA = within plate alkalic basalt; WPT = within plate tholeiite.

fractionation by normalizing to  $^{88}\text{Sr}/^{86}\text{Sr} = 8.375209$  and  $^{146}\text{Nd}/^{144}\text{Nd} = 0.7219$ , respectively. The international standard samples, NBS-987 and JNdi-1, were employed to evaluate instrument stability during the period of data collection. The measured values for the NBS-987 Sr standard and JNdi-1 Nd standard were  $^{87}\text{Sr}/^{86}\text{Sr} = 0.710267 \pm 0.000011$  ( $n = 8$ ;  $2\sigma$ ) and  $^{143}\text{Nd}/^{144}\text{Nd} = 0.512111 \pm 0.000013$  ( $n = 7$ ;  $2\sigma$ ), respectively. U.S. Geological Survey reference material BCR-2 was measured to monitor the accuracy of the analytical procedures, with the following results:  $^{87}\text{Sr}/^{86}\text{Sr} = 0.705037 \pm 0.000010$  ( $n = 2$ ;  $2\sigma$ ) and  $^{143}\text{Nd}/^{144}\text{Nd} = 0.512624 \pm 0.000015$  ( $n = 2$ ;  $2\sigma$ ). The  $^{87}\text{Sr}/^{86}\text{Sr}$  and  $^{143}\text{Nd}/^{144}\text{Nd}$  data of BCR-2 show good agreement with previously published data by thermal ionization mass spectrometer and multicollector-inductively coupled plasma-mass spectrometry techniques (Li et al., 2011).

## 6. Results

### 6.1. Mineral Chemistry

Representative electron microprobe analyses of clinopyroxenes in mafic rocks are listed in Table S1 in the supporting information. Clinopyroxenes from massive basalts are entirely diopsides ( $\text{Wo}_{47-49}\text{En}_{41-46}\text{Fs}_{7-10}$ ) with  $\text{Mg}^{\#} = 80-86$  (Table S1 and Figure 10a). They have high CaO contents of 23.0–24.0 wt.% and low  $\text{Al}_2\text{O}_3$  (1.52–3.25 wt.%) and FeO (4.71–6.41 wt.%) contents. The clinopyroxenes from a dolerite dyke are diopsides ( $\text{Wo}_{47-48}\text{En}_{45-47}\text{Fs}_{5-8}$ ) with  $\text{Mg}^{\#} = 86-90$  and augites ( $\text{Wo}_{39-42}\text{En}_{38-47}\text{Fs}_{14-20}$ ) with  $\text{Mg}^{\#} = 65-77$  (Table S1 and Figure 10a). Diopsides are similar to those from the massive basalt. The augites have low CaO contents of 18.8–19.6 wt.% and high  $\text{Al}_2\text{O}_3$  (2.17–3.97 wt.%) and FeO (8.78–12.1 wt.%) contents. Clinopyroxene phenocrysts in pillow basalt are diopsides ( $\text{Wo}_{47-48}\text{En}_{41-47}\text{Fs}_{5-11}$ ) with  $\text{Mg}^{\#} = 80-90$  (Table S1 and Figure 10a), but the groundmass of pillow basalt also contains diopsides ( $\text{Wo}_{48-49}\text{En}_{37-42}\text{Fs}_{11-14}$ ) with  $\text{Mg}^{\#} = 73-80$  and augites ( $\text{Wo}_{28-35}\text{En}_{40-43}\text{Fs}_{24-30}$ ) with  $\text{Mg}^{\#} = 57-64$  (Table S1 and Figure 10a). Compared to phenocrysts, groundmass diopsides have relatively low  $\text{Al}_2\text{O}_3$  (2.07–2.08 wt.%) contents but high FeO (6.54–8.60 wt.%) contents. Augites from massive basalt have lower CaO contents of 12.2–15.4 wt.% and high FeO contents of 13.3–16.5 wt.%. Clinopyroxenes from dolerite slice are all augites ( $\text{Wo}_{40-45}\text{En}_{38-43}\text{Fs}_{17-20}$ ) with  $\text{Mg}^{\#} = 66-71$  (Table S1 and Figure 10a). They have high  $\text{TiO}_2$  contents (0.80–1.98 wt.%),  $\text{Al}_2\text{O}_3$  (2.39–5.59 wt.%), and FeO (10.2–12.2 wt.%).

Clinopyroxenes compositions in mafic rocks are an effective tool for classifying tectonic settings (Nisbet & Pearce, 1977). In general, the clinopyroxenes from dolerite slices have high  $\text{TiO}_2$ , FeO, and MnO contents relative to those from the massive basalts and dolerite dykes (Table S1) and they resemble OIBs. On a discriminant diagram (Figure 10b), the clinopyroxenes from the massive basalt plot within the volcanic arc basalt (VAB) field and those from dolerite dykes plot in the VAB and ocean floor basalt (OFB) fields. However, clinopyroxenes from the pillow basalts and dolerite slices plot within VAB, OFB, and within plate tholeiite (WPT) fields. Collectively, these signatures indicate development in a SSZ environment.

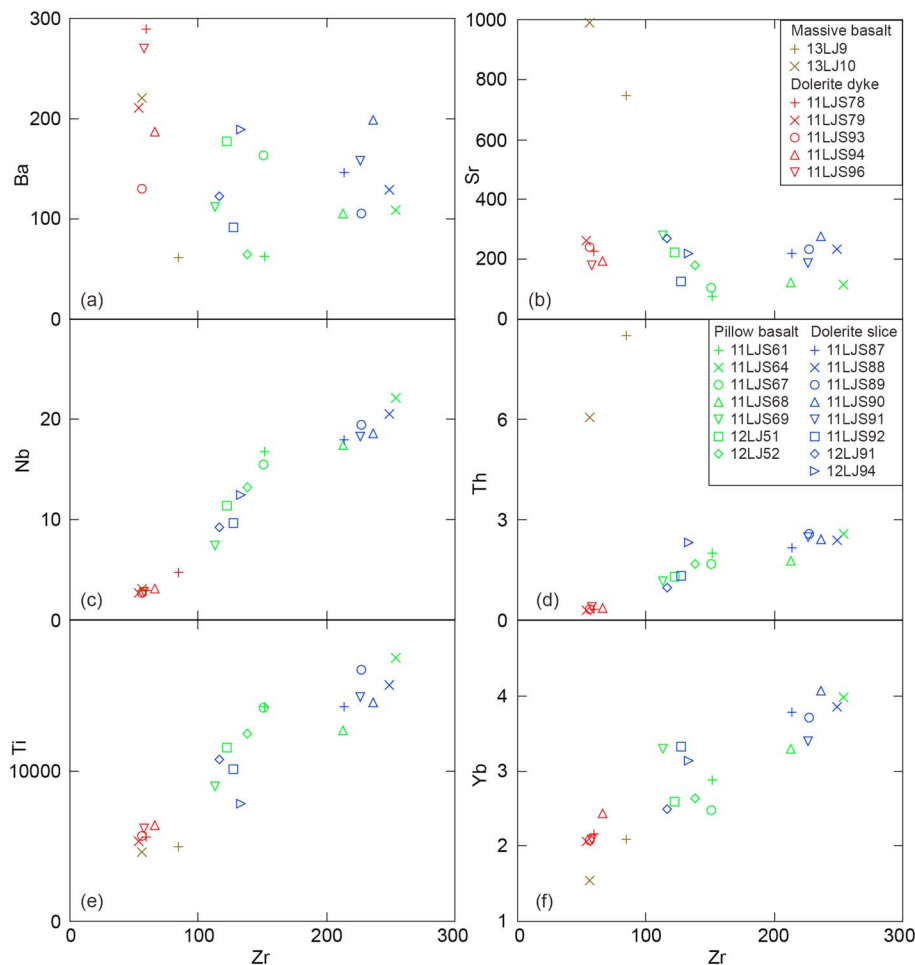


**Figure 11.** (a–f) Variations of selected trace elements of mafic rocks from the Lajishankou ophiolite complex.

## 6.2. Major and Trace Elements

Twenty-two samples, including two massive basalts, five dolerite dykes, seven pillow basalts, and eight dolerite slices, were analyzed for major and trace element concentrations. The analytical results are listed in Table S2, and all concentrations are expressed in weight percent for major elements and ppm for REEs and trace elements. Variable loss on ignition values (1.27–4.39 wt.%) in mafic rocks reflect secondary alteration, which is indicated by presence of mineral phases (e.g., epidote, calcite, and chlorite; Figures 9b and 9e). As low-grade alteration may lead to selective element mobility (Pearce & Cann, 1973). When plotted against Zr (immobile element), large ion lithophile elements (LILE; e.g., Sr, K, and Rb) show scattered distribution, whereas immobile high field strength elements (HFSE) and REE display well-defined trends (Figure 11). Therefore, relatively immobile elements such as Th, Nb, Zr, Ti, V, and REE are used in the discussion that follows to characterize the mafic rocks with respect to their original composition and possible tectonic settings (Pearce, 2008, 2014; Shervais, 1982).

On the basis of Zr/Ti versus Nb/Y diagram, all samples have subalkaline compositions (Figure 12a). Except for three altered samples with high SiO<sub>2</sub> contents that probably result from SiO<sub>2</sub> addition during alteration (Pearce, 2014), most belong to tholeiitic basalts on the FeO<sup>T</sup>/MgO versus SiO<sub>2</sub> diagram (Figure 12b). The major element concentrations of massive basalts are constant overall, with 47.0–48.1 wt.% SiO<sub>2</sub>, 6.08–8.55 wt.% MgO, 10.2–11.5 wt.% FeO<sup>T</sup>, and 0.77–0.82 wt.% TiO<sub>2</sub> (Table S2). Chondrite-normalized REE patterns are right inclined and enriched in light REE (LREE; La<sub>N</sub>/Yb<sub>N</sub> = 9.23–9.41; Figure 13a). The massive basalts display weak to negligible negative Eu anomalies (Eu/Eu\* = 0.87–0.90), strong enrichment in Th and apparent depletion in Nb, Ta, Zr, Hf, and Ti (Figure 13b). Such features are typical of island arc rocks (Pearce & Peate, 1995).



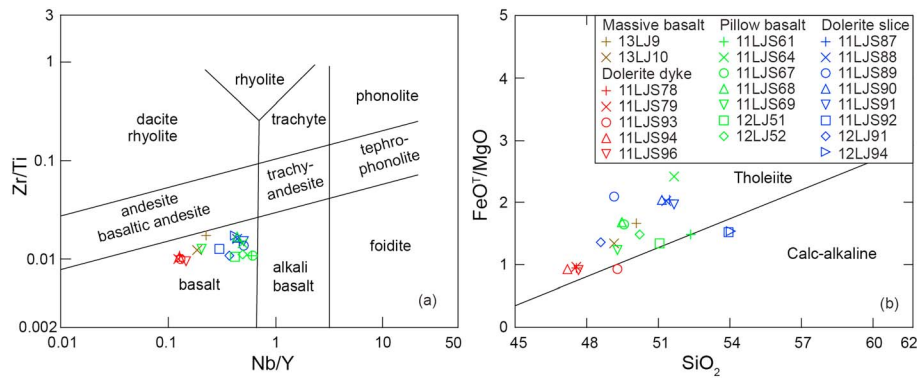


**Figure 12.** (a) Zr/Ti versus Nb/Y diagram (after Pearce, 2014) and (b) SiO<sub>2</sub> versus FeO<sup>T</sup>/MgO diagram (after Miyashiro, 1974) of mafic rocks from the Lajishankou ophiolite complex.

Dolerite dykes have low SiO<sub>2</sub> (45.3–47.2 wt.%), TiO<sub>2</sub> (0.89–1.06 wt.%), and FeO<sup>T</sup> (8.66–10.4 wt.%) contents along with high MgO (9.33–11.1 wt.%) contents (Table S2). They are distinctly different from other mafic rocks with nearly flat chondrite-normalized REE patterns ( $La_N/Yb_N = 1.12\text{--}1.20$ ; Figure 13a). These dolerite dykes have insignificant positive Eu anomalies ( $Eu/Eu^* = 1.04\text{--}1.11$ ) and slight depletion in Nb and Ti (Figure 13b). Immobile element patterns normalized to N-MORB reveal that the dolerite dykes have similar geochemical characteristics to back-arc basin basalts (BABBs) (Figure 13b; Pearce et al., 2005).

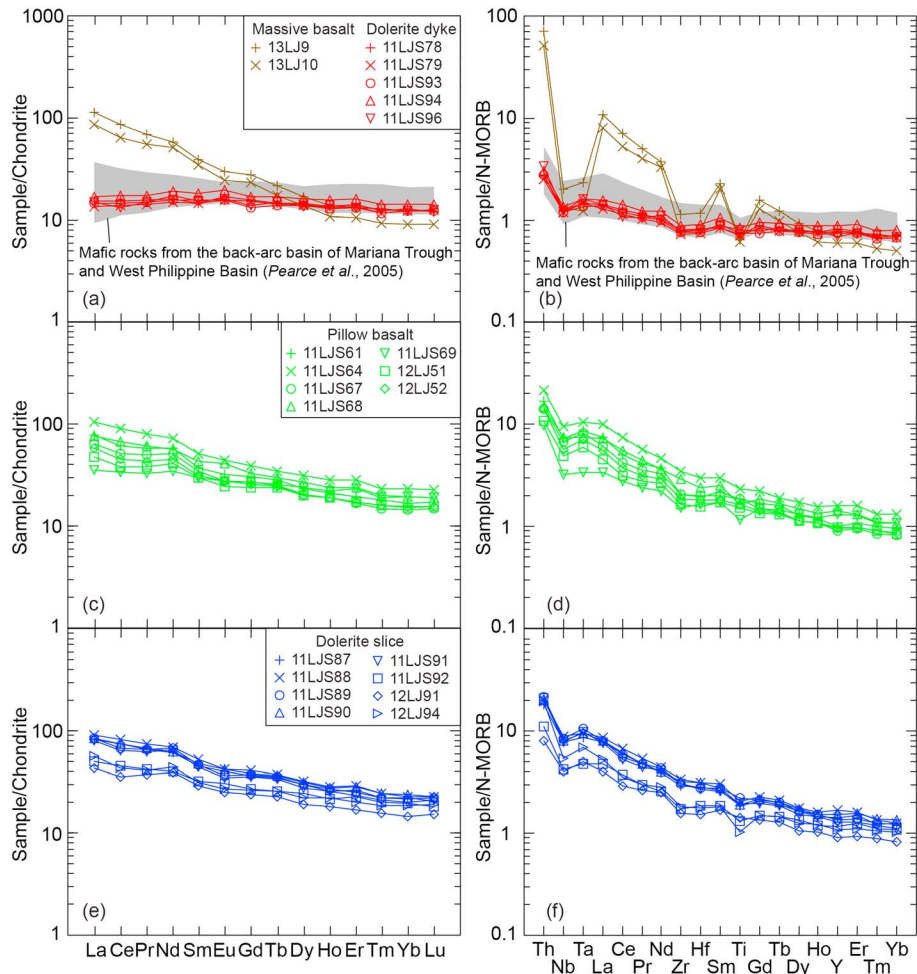


**Figure 13.** (a, c, and e) Chondrite-normalized rare earth element patterns and (b, d, and f) N-MORB-normalized trace element patterns of the mafic rocks from the Lajishankou ophiolite complex. Chondrite and normal mid-ocean ridge basalt data are from Sun and McDonough (1989).

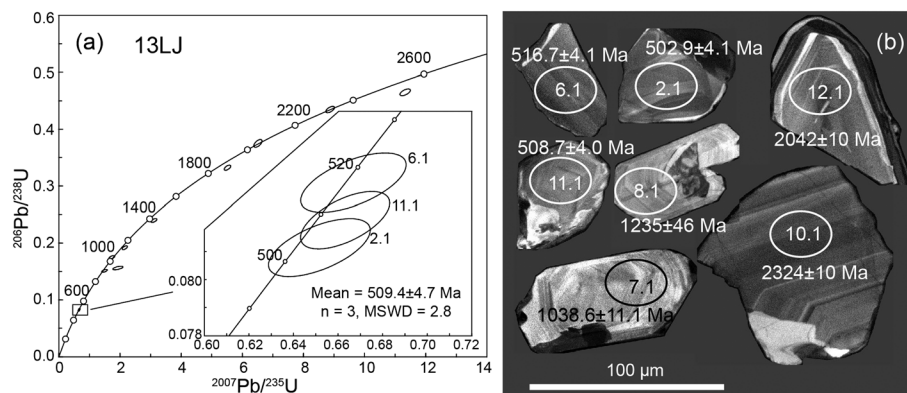


**Figure 14.** (a) Zircon SHRIMP U-Pb concordia diagram and (b) cathodoluminescence images for zircons from dolerite dyke (13LJ) collected from the Lajishankou ophiolite complex. MSWD = mean square weighted deviate.

The pillow basalts and dolerite slices have similar major and trace element concentrations. SiO<sub>2</sub> ranges from 46.9 to 52.5 wt.%, with high TiO<sub>2</sub> (1.30–2.92 wt.%) contents. FeO<sup>T</sup> and MgO range widely from 8.98 to 13.1 wt.% and from 5.43 to 8.05 wt.%, respectively (Table S2). They are enriched in LREE with right-inclined REE patterns (La<sub>N</sub>/Yb<sub>N</sub> = 1.81–4.61; Figures 13c and 13e). Pillow basalts and dolerite slices show negligible Eu anomalies (Eu/Eu\* = 0.87–1.08) and slight depletion in Nb and Ti (Figures 13d and 13f). Their N-MORB-normalized immobile element patterns are akin to OIB-like rocks (Figures 13d and 13f; Pearce et al., 2005).

In summary, geochemical data demonstrate compositional heterogeneity among mafic rocks in the Lajishankou ophiolite complex. Compositional variation may result from crystal fractionation and increasing degree of melting of their mantle source; however, trace element and Sr-Nd isotopic data suggest the influence of different mantle sources.

### 6.3. Zircon U-Pb Ages

Typical CL images of zircons from the dolerite dyke are presented in Figure 14b. The analytical data are listed in Table S3. All zircons from the dolerite dyke (13LJ) are transparent and colorless, with variable shapes, sizes, and internal structures. Three smaller zircons are fragmentary grains with lengths of 60–70 µm. Their CL images exhibit patchy and broad-spaced zoning texture (Figure 14b), resembling magmatic zircons in gabbro. The larger zircons are euhedral with lengths of 70–100 µm. Their CL images show regular oscillatory magmatic zonings, with some of them displaying dark inherited cores (Figure 14b).

Twelve zircon grains with different internal structures were analyzed by SHRIMP II and yield concordant ages ranging between 502.9 ± 4.1 Ma (<sup>206</sup>Pb/<sup>238</sup>U age) and 2622 ± 9 Ma (<sup>207</sup>Pb/<sup>236</sup>U age) (Table S3). Three zircons with broad-spaced zoning textures have relatively high and consistent U and Th concentrations (U = 445–488 ppm and Th = 175–301 ppm) resulting in high Th/U ratios of 0.41–0.64 (Table S3) and yield a weighted mean <sup>206</sup>Pb/<sup>238</sup>U age of 509.4 ± 4.7 Ma (mean square weighted deviate = 2.8; Figure 14a), representing the age of magmatic crystallization. However, the other nine zircons with low U and Th concentrations (U = 101–356 ppm and Th = 47–263 ppm) and Th/U ratios of 0.19–0.77 yield concordant ages older than 900 Ma ranging between 906.9 ± 9.1 Ma (<sup>206</sup>Pb/<sup>238</sup>U age) and 2622 ± 9 Ma (<sup>207</sup>Pb/<sup>236</sup>U age) (Table S3). These inherited zircons with variable shapes were possibly transported as detrital grains into the mantle wedge via subduction of oceanic crust.

In addition, SHRIMP zircon U-Pb dating of a dolerite slice sample yielded a weighted mean <sup>206</sup>Pb/<sup>238</sup>U age of 491.0 ± 5.1 Ma (*n* = 10; mean square weighted deviate = 1.6) without inherited grains (Fu et al., 2014), which is slightly younger than the dolerite dyke.

### 6.4. Sr-Nd Isotopes

Eight whole-rock samples were analyzed for Sr and Nd isotopic compositions. The results are listed in Table S4 and plotted in Figure 15a. Initial isotopic ratios of the mafic rocks are calculated based on their zircon ages. The intrusive contact relationship between the dolerite dyke and massive basalt indicates that the massive basalts may have formed at circa 514 Ma (age of Cambrian island arc felsic rock; Figure 3) earlier than

dolerite dyke ( $509.4 \pm 4.7$  Ma). Similar geochemistry and Sr-Nd isotopes of pillow basalt and dolerite slice indicate that they were probably coeval and formed at  $491.0 \pm 5.1$  Ma (Fu et al., 2014).

Dolerite dykes and slices have low initial  $^{87}\text{Sr}/^{86}\text{Sr}$  ratios ( $I_{\text{Sr}}$ ) ranging from 0.70336 to 0.70428 (Table S4), but massive basalts and pillow basalts have high initial  $^{87}\text{Sr}/^{86}\text{Sr}$  ratios ( $I_{\text{Sr}}$ ) of 0.70441–0.70443 and 0.70531–0.70534 (Table S4), respectively. The Sr isotopic compositions of mafic rocks could be modified by seawater alteration and drift away from mantle array (Nohda et al., 1992). Thus, the high initial  $^{87}\text{Sr}/^{86}\text{Sr}$  ratios ( $I_{\text{Sr}} > 0.704$ ; Figure 15a) of basalts probably indicate strong alteration related to interaction with seawater (Nohda et al., 1992). However, the Nd isotopic compositions were relatively stable despite a significant change in Sr isotopic values (Figure 15a). All mafic rocks have positive  $\epsilon_{\text{Nd}}(t)$  values. The  $\epsilon_{\text{Nd}}(t)$  values of massive basalts and dolerite dykes are +6.0 to +6.6 and +6.1 to +6.3, respectively, but pillow basalts and dolerite slices have lower  $\epsilon_{\text{Nd}}(t)$  values (+5.2 to +5.8 and +4.8 to +5.3). This variation suggests that the pillow basalts and dolerite slices might have been affected by the input of enriched component.

## 7. Discussion

### 7.1. Geodynamic Setting

New petrological, mineralogical, geochemical, and geochronological data from mafic rocks of the Lajishankou ophiolite complex can be used to discriminate three distinct lithological assemblages that formed in different, but not incompatible, tectonic settings with different mantle sources. Massive tholeiitic basalts (Group 1) with strong enrichment in Th and LILE but depletion of HFSE (e.g., Nb, Ta, Zr, Hf, and Ti; Figures 13a and 13b) may have developed in an island arc environment characterized by contamination of their mantle source by dehydration of subducting oceanic crust which led to partial melting and LILE enrichment of the overlying mantle wedge (Ishizuka et al., 2007; Manikyamba et al., 2015; Pearce, 2014; Pearce & Peate, 1995). This inference is further supported by clinopyroxene compositions (Figure 10b; Nisbet & Pearce, 1977). Clinopyroxenes of massive basalts plot within the VAB field, whereas those of dolerite dykes (Group 2) fall within the VAB and OFB fields. Dolerite dykes also display nearly flat chondrite-normalized REE patterns without obvious anomalies, suggesting a possible back-arc basin environment (Ishizuka et al., 2010; Pearce et al., 2005). Pillow basalts and dolerite slices (Group 3) are characterized by enrichment of LILE, LREE, and HFSE relative to island arc basalts and BABBs (Figures 13c–13f). They also have high  $\text{TiO}_2$  contents (1.30–2.92 wt.%) and low LREE/HFSE and Zr/Nb (9.05–15.3) ratios, which are different from lavas erupted at destructive plate boundaries but somewhat similar to OIB (Weaver, 1991). Clinopyroxenes from dolerite slices with high  $\text{TiO}_2$  (0.80–1.98 wt.%) and FeO (10.2–12.2 wt.%) contents are more akin to those from WPTs (Nisbet & Pearce, 1977). However, clinopyroxenes of pillow basalts are geochemically variable and fall within the VAB, OFB, and WPT fields, indicating a possible range of magmatic sources. In addition, spinels in serpentinites are characterized by relatively high  $\text{Cr}_2\text{O}_3$  contents of 47.5–50.6 wt.% and low contents of  $\text{Al}_2\text{O}_3$  (14.3–17.6 wt.%) and MgO (7.17–10.2 wt.%) with  $\text{Cr}^\# = 64\text{--}69$  and  $\text{Mg}^\# = 37\text{--}50$ , suggesting a SSZ origin (Fu & Yan, 2017).

In order to further evaluate their geodynamic setting, the analyzed samples are plotted on trace element discrimination diagrams (Figures 15c and 15d). In general, island arc basalts, mid-ocean ridge basalts, and OIBs have distinct Ti/V ratios (Shervais, 1982). Thus, a Ti/V versus Zr discrimination diagram provides an effective means of discriminating basalts from different tectonic environments (Manikyamba et al., 2015). Massive basalt and dolerite dyke samples with low Ti/V ratios plot within the island arc basalt and BABB fields, respectively (Figure 15c), but pillow basalt and dolerite slice samples with high Ti/V ratios mainly fall within the OIB field. Pearce (2014) applied the Th/Yb versus Nb/Yb diagram (Figure 15d) to identify lavas from nonsubduction settings or SSZ environment. Due to the addition of subduction-related melt to the mantle wedge, lavas in SSZs are variably displaced from MORB-OIB array to higher Th/Yb. The massive basalt samples fall into the fields associated with intraoceanic arc (Figure 15c). Their high Th/Yb ratios (3.94–4.07) can be explained by mixing with melt derived from subducted sediment (Pearce, 1982). Dolerite dyke samples are slightly displaced from MORB-OIB array and plot within the BABB field. Pillow basalt and dolerite slice samples mainly fall into the OIB field and are also slightly displaced from that array (Figure 15d).

Indeed, VABs and BABBs are dominant during the evolution of intraoceanic arc-basin systems (Ishizuka et al., 2009; Stern et al., 2003). The distinct compositions of massive basalts (Figures 13a, 13b, 15c, and 15d) coupled



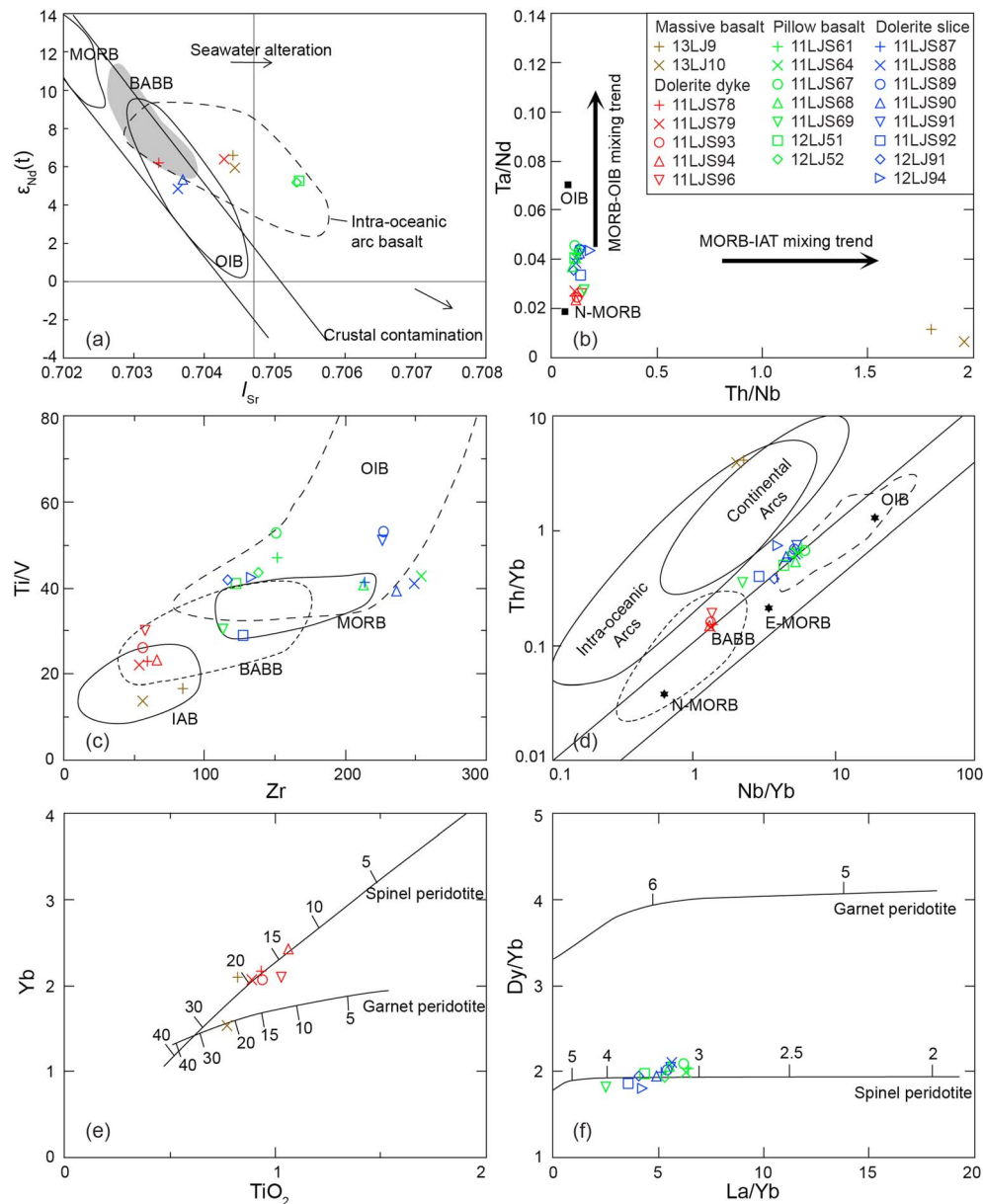


**Figure 15.** (a)  $\epsilon_{Nd}(t)$  versus  $I_{Sr}$  diagram of the mafic rocks. (b) Ta/Nd versus Th/Nb diagram of mafic rocks (after Aldanmaz et al., 2008). (c) Ti/V versus Zr diagram (after Manikyamba et al., 2015) and (d) Th/Yb versus Nb/Yb diagram (after Pearce, 2008) of mafic rocks from the Lajishankou ophiolite complex. (e)  $TiO_2$  versus Yb (after Gribble et al., 1996) and (f) Dy/Yb versus La/Yb (after Jung et al., 2006) diagrams for mafic rocks at Lajishankou. BABB = back-arc basin basalt; MORB = mid-ocean ridge basalt; OIB = ocean island basalt; IAB = island arc basalt.

with their Sr-Nd isotopes (Figure 15a) probably reflect an intraoceanic arc environment. Although dolerite dykes are indistinguishable from N-MORBs on the basis of trace element patterns, an intrusive contact with VAB (Figures 8a and 8b) coupled with clinopyroxene of VAB affinity (Figure 10b) indicates formation in a SSZ environment. We note here that OIB-type lavas without plume involvement have been reported from back-arc basins (Hickey-Vargas et al., 2006; Ishizuka et al., 2009). Pillow basalts and dolerite slices have OIB-like enriched LREE patterns (Figures 13c–13f). In addition, interbedded limestone also occurs within these pillow basalts (Figure 8d). Thus, we suggest that those mafic rocks may have originated from seamounts in a back-arc basin.

Moreover, the SSZ affinity of the Lajishankou ophiolite complex is consistent with the results of structural and petrological investigations that indicate it developed in the upper plate of the subduction zone.

## 7.2. Mantle Source Characteristics

Mafic rocks from the Lajishankou ophiolite complex appear to have formed in a SSZ setting. The chemical compositions of magmas in SSZ are mainly controlled by mixing of the depleted mantle wedge, subducted sediment, and altered oceanic crust (Elliott, 2003; Pearce & Peate, 1995; Taylor & Nesbitt, 1998). Massive basalts have pronounced positive Th, P, and LREE anomalies and high La/Sm and Th/Nb ratios (Figure 15b), which are diagnostic features attributable to sediment addition to the mantle wedge in a typical intraoceanic arc setting (Elliott, 2003; Manikyamba et al., 2015; Pearce & Peate, 1995). Their lower  $\epsilon_{\text{Nd}}(t)$  values (+6.0 to +6.6) are consistent with intraoceanic arc basalt (Figure 15a) and also indicate sediment addition to the mantle wedge (Ishizuka et al., 2007; Stern et al., 2003). In addition, massive basalts have a relatively higher REE contents, probably indicating that their magmas were generated from less depleted mantle sources. Gribble et al. (1996) used Yb versus  $\text{TiO}_2$  diagram to estimate the composition of mantle sources and the degree of partial melting that generates different magmas in intraoceanic arc-basin system. The diagram shows that massive basalts were derived from high degrees (21–27%) of spinel peridotite melting (Figure 15e), reflecting an arc-like source and hydrous melting of the mantle wedge (Gribble et al., 1998).

Dolerite dykes are characterized by high Zr/Nb (19.5–20.9), Y/Nb (6.84–8.0), and low Zr/Y (2.43–3.01) ratios and similar  $\epsilon_{\text{Nd}}(t)$  values (+6.1 to +6.3) with BABBs (Figure 15a), suggesting that a depleted mantle source has been involved in their magma formation. Their N-MORB-like trace element patterns further indicate that their source region experienced a previous melt extraction (Woodhead et al., 1993). Taking into account inherited Proterozoic zircons and relatively high Th/Yb ratios at a given Nb/Yb (Figure 15d), their MORB-like mantle may have been influenced by subduction-related processes in terms of slab dehydration and slab melting. Their magmas can be accounted for by melts generated from low degrees (13–20%) of decompression melting of MORB-like mantle beneath back-arc basins (Figure 15e; Gribble et al., 1998).

In contrast to the massive basalts and dolerite dykes, lower Zr/Nb, Y/Nb, and higher Zr/Y ratios of the OIB-like pillow basalts and dolerite slices (9.05–15.3, 1.65–4.93, and 3.10–6.28, respectively) can be attributed to a more enriched source and/or generation under smaller degrees of partial melting (Hickey-Vargas et al., 2006; Ishizuka et al., 2009). Their lower  $\epsilon_{\text{Nd}}(t)$  values (+4.8 to +5.8; Figure 15a) at Th/Ce < 0.1 (0.04–0.09) and increasing Ta/Nd ratios at near constant Th/Nb (Figure 15b) confirm a contribution of enriched source to MORB-like mantle beneath back-arc basins (Aldanmaz et al., 2008; Ishizuka et al., 2009). In addition, the weak fractionation of HREE (Dy/Yb = 1.8–2.1) suggests that the primitive lavas represent partial melts of spinel peridotite (Figure 15f).

## 7.3. Implications for Tectonic Evolution

The Proto-Tethyan Ocean is commonly interpreted to have been subducted beneath the Central Qilian block during the Cambrian with 530- to 480-Ma SSZ-type ophiolites and arc-related volcanic rocks having formed within a marginal ocean basin before being accreted to the southern margin of the Central Qilian block (Fu et al., 2014; Fu & Yan, 2017; Huang et al., 2015; Qiu et al., 1997; Song et al., 2014; C. Wang et al., 2017; Yan et al., 2015; J. X. Zhang, Yu, & Mattinson, 2017). However, models involving ubiquitous subduction beneath continental margins create tectonic conundrums when juvenile, intraoceanic terranes are identified within and juxtaposed against continental crustal fragments. The difficulties arise because oceanic crust situated on the downgoing slab is rarely preserved on continental margins (Brown et al., 2011; Yamamoto et al., 2009). Rather, ophiolites and island arc complexes are more readily preserved on the overriding plate in a suprasubduction setting and are later thrust over a continental margin, which remains attached to the downgoing oceanic crust as it is subducted beneath the intraoceanic arc system (Brown et al., 2011; Clift & Vannucchi, 2004). This is well documented in modern day arc-continent collisions such as Taiwan where the Luzon arc is currently colliding with the continental mass of Eurasia via east dipping subduction in the south but is undergoing subduction flip along the Okinawa trough to the NE (Boutelier & Chemenda, 2011; Clift et al., 2003). These types of arc-continent collisions associated with subduction flips are also recognized in Paleozoic Tasmanides of eastern Australia as discrete “quantum” additions of juvenile oceanic crust including the Ordovician Macquarie Arc in the Lachlan Orogen and the Devonian Gamilaroi terrane and Permian Gympie terrane in the New England Orogen (Aitchison & Buckman, 2012). Andean-type margins involving continuous subduction beneath a continent are less likely to preserve any significant oceanic crustal material within the orogen apart from relatively small volumes of upper volcanic and sedimentary portions shaved off and into the accretionary complex during subduction (Clift & Vannucchi, 2004; Yamamoto et al., 2009). Our



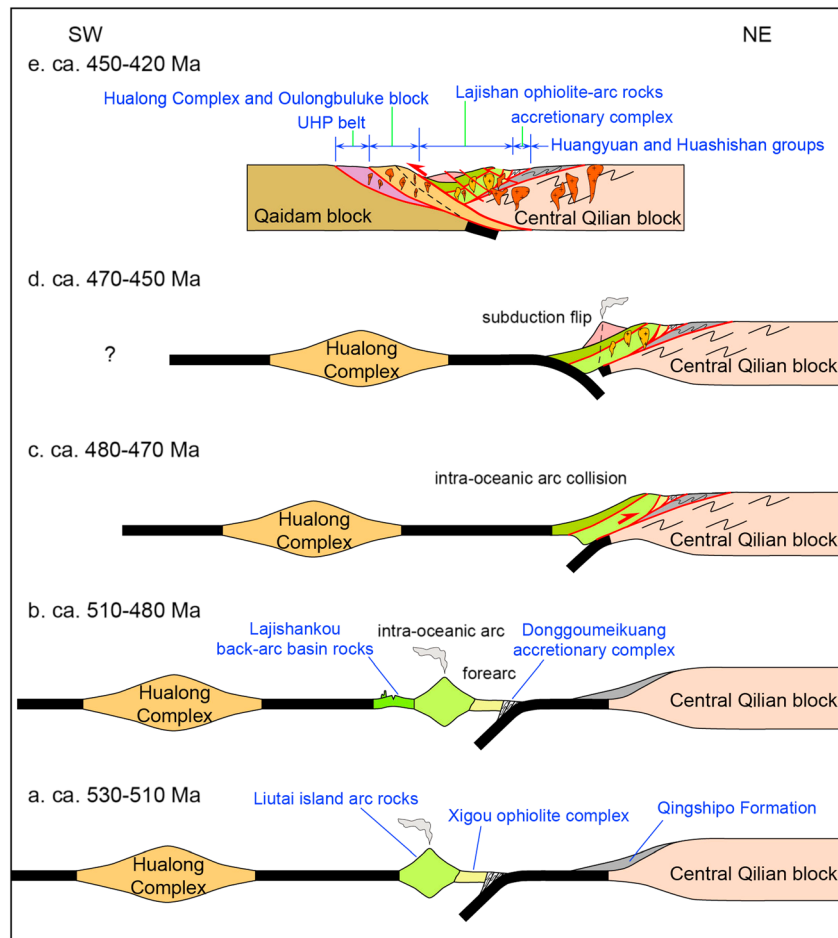


**Figure 16.** Tectonic model for evolution of Lajishan ophiolite-arc rocks. (a) Subduction of the Proto-Tethyan Ocean and generation of accretionary complex, fore-arc ophiolite, and intraoceanic arc. (b) Intraoceanic arc-basin system with back-arc spreading. Seamount formed in a back-arc basin. (c) Emplacement of the Lajishan ophiolite-arc rocks onto the Central Qilian block. (d) Renewed subduction with opposite polarity and construction of a 470- to 450-Ma continental arc (after Yan et al., 2015). (e) Closure of Proto-Tethyan Ocean and collision between Qaidam, Oulongbuluke, South Qilian, and Central Qilian blocks. Circa 450- to 420-Ma postcollisional magmatism is in response to deep subduction of the Qaidam block.

geological mapping and new data from the Lajishankou ophiolite complex suggest that it incorporates three different compositional groups. They represent different types of magmas (island arc tholeiite [IAT], BABB, and OIB) generated during distinct stages in the evolution of an intraoceanic arc-basin system (Figures 16a and 16b). The exact mechanism by which these intraoceanic rocks have been incorporated into the Central Qilian belt is difficult to reconcile. However, as they have such distinct intraoceanic signatures and rarely exceed subgreenschist facies metamorphism this suggests that the Lajishan ophiolite-arc rocks probably formed far from any continental influence. Structural and geological cross sections across the Lajishan ophiolite complex are consistent with the interpretation that it originated in the upper plate of the subduction zone and was thrust over the Neoproterozoic-Ordovician Qingshipo Formation, which together with the Huashishan Group, was also thrust over the Neoproterozoic basement of Central Qilian block (Figures 1c, 2, 3, and 5; Guo & Li, 1999). The arc-continent collision responsible for their preservation potentially involved a more complex series of subduction flips in order to preserve the juvenile oceanic crustal elements as subgreenschist facies rocks in an upper plate position juxtaposed against Proterozoic gneisses and schists of the Hualong Complex and Central Qilian block (Figure 16).

Between circa 530 and 510 Ma, a Cambrian intraoceanic subduction system, consisting of Donggoumeikuang accretionary complex, Xigou ophiolite, and Liutai island arc, had developed in the Proto-Tethyan Ocean (Figure 16a). The Donggoumeikuang accretionary complex is mainly composed of pillow basalts, radiolarian chert, limestone, and turbiditic sandstone (Figure 3). To the south of the

accretionary complex, the Xigou ophiolite consists of boninites and peridotites with mid-ocean ridge and SSZ affinities (Fu & Yan, 2017; Smith & Yang, 2006), which are similar to the rock assemblages from the Mariana forearc (Parkinson et al., 1992). Then, Liutai island arc rocks, including volcanoclastic rocks, andesites, dacites, and rhyolites (Fu & Yan, 2017; Qiu et al., 1997), erupted in an intraoceanic arc setting. In the Lajishankou ophiolite complex, massive basalts with IAT affinity and positive  $\epsilon_{\text{Nd}}(t)$  values also indicate an intraoceanic arc environment (Figures 10b, 15a, 15c, and 15d). Associated magmas are characterized by high degrees of partial melting of arc-type mantle, modified by subduction components (Figures 15a and 15b). The spatial distribution of Liutai island arc rocks, Liutai ophiolite complex, and Donggoumeikuang accretionary complex from the south to the north (Figures 1c, 3, 4a–4c, and 16) suggest the southward subduction of Proto-Tethyan Ocean (Figure 16a).

Around 510 Ma, rifting of the intraoceanic arc generated an oceanic back-arc basin, similar to Mariana back-arc basin (Figure 16b). The development of an upwelling MORB-like mantle flow regime is required during the extension of a back-arc basin. Due to the interaction between MORB-like and arc-like mantle components, lavas of either these affinities may have erupted during the early stages of back-arc rifting (Gribble et al., 1998; Manikyamba et al., 2015). Geochemical data from dolerite dykes indicate intrusion within a back-arc basin with a detectable influence of SSZ components (Figures 10b, 15c, and 15d).

From 510 to 480 Ma, southward subduction of the Proto-Tethyan Ocean ensued and the intraoceanic arc-basin system continued to develop (Figure 16b). Island arc rocks consisting of abundant basalts, andesites, dacites, and rhyolites were erupted as a result of active arc-related magmatism in the Late Cambrian (Qiu et al., 1997). Meanwhile, OIB-like pillow basalts and dolerite with little evidence of any subduction signature also formed (Figures 10b, 15c, and 15d). OIB-like rocks with intercalated limestones confirm the existence of seamounts within the back-arc basin.

Between 480 and 470 Ma, southward subduction of the Proto-Tethyan Ocean along the southern margin of the Central Qilian belt continued. Subsequently, the oceanic island arc, which included SSZ ophiolites, back-arc basin, and accretionary complex elements collided with the Central Qilian block and was obducted over the Qingshipo Formation, resulting in formation of a series of NE vergent imbricated thrust sheets along the southern margin of Central Qilian block (Figures 1c, 2, and 16c). The timing of arc-continent collision is constrained at 480–470 Ma, which represents the interval between the youngest age of Lajishan ophiolite (Fu & Yan, 2017) and the oldest age of granitoid intrusions, respectively.

Subduction resumed from circa 470–450 Ma but with the opposite polarity. This generated the 470- to 450-Ma continental arc in the Lajishan and Central Qilian areas (Figure 16d) (Fu & Yan, 2017; C. Wang et al., 2017; Yan et al., 2015). This interpretation is supported by the presence of a voluminous Ordovician andesite, dacite, rhyolite, pyroclastic rocks, and volcanoclastic sandstones around Lajishan (BGMRQP, 1964; Feng et al., 2002; Qiu et al., 1997). In addition, SW vergent thrust faults (Figures 1c and 2) developed and voluminous coeval granitoids with continental arc affinity intruded the ophiolite and island arc in the Lajishan area (Figures 1c, 2, and 5) and Precambrian metamorphic rocks in the Central Qilian block (C. Wang et al., 2017; Xiao et al., 2009). These indicate northward subduction of the Proto-Tethyan Ocean along the southern margin of the Neoproterozoic Central Qilian block.

From circa 450–420 Ma, the Proto-Tethyan Ocean was closed and microcontinents collided (Figure 16e) by the end of Ordovician (Song et al., 2014; Xia et al., 2016; J. X. Zhang, Yu, & Mattinson, 2017). Voluminous 450–420 Ma syncollisional and postcollisional granitoids intruded into the Hualong Complex and Central Qilian block (Huang et al., 2015; C. Wang et al., 2017; Yan et al., 2015; Yang et al., 2016). Between 450 and 410 Ma the Neoproterozoic Hualong Complex experienced metamorphism and deformation (Yan et al., 2015, and references therein). Together with Qaidam and Oulongbuluke blocks, it is likely to have accreted to the north and amalgamated with the Central Qilian block before circa 450 Ma (Figure 16e). Thus, a broad zone of 450–420 Ma postcollisional magmatism occurred along the North Qaidam UHP belt, Central Qilian, South Qilian, and Oulongbuluke blocks (Huang et al., 2015; C. Wang et al., 2017; Xia et al., 2016; Yan et al., 2015; Yang et al., 2016). A 440- to 420-Ma peak UHP metamorphic age has been obtained from coesite-bearing metapelites and eclogites and diamond-bearing garnet peridotites in the North Qaidam accretionary complex (Song et al., 2014; Xia et al., 2016; J. X. Zhang, Yu, & Mattinson, 2017, and references therein). These rocks are thought to have developed in response to deep subduction of the Qaidam block.



## 8. Conclusions

1. The Lajishankou ophiolite complex along the northern margin of the South Qilian belt consists of various tectonic slices, including serpentinite, wehrlite, pyroxenite, gabbro, dolerite, and pillow and massive basalts, which were thrust onto a passive margin sequence consisting of alternating turbiditic sandstones and mudstones deposited on the Central Qilian block.
2. Mafic rocks associated with the Lajishankou ophiolite complex are of three main types: massive IATs, back-arc dolerite dykes, and pillow basaltic and dolerite slices that are also of back-arc affinity.
3. The Lajishan ophiolite complex formed within an intraoceanic arc-basin system at circa 530–480 Ma that was located above a southward subducting slab of Proto-Tethyan oceanic lithosphere. This intraoceanic arc system was emplaced onto the Central Qilian block during the Early Ordovician.
4. Arc-continent collision was followed by a subduction flip and the development of a continental “Andean-type” convergent margin accompanied by intrusion of Cordilleran batholiths in the Middle Ordovician.
5. Collision of the Hualong Complex resulted in 450- to 420-Ma postcollisional magmatism within the Hualong Complex and Central Qilian block.

## Acknowledgments

We thank Zhenyu Chen and Chaofeng Li for help in obtaining the microprobe and Sr-Nd isotope data. We also thank Chun Yang and Liqin Zhou for mounting and CL imaging of zircons, and Wei Zhang for SHRIMP measurements. The study was funded by the National Natural Science Foundation of China (41672221, 41702239, 41372207, and 41272221) and Key China Geological Survey (DD20160201-04 and DD20160022-02). We are also grateful to Editor, Nathan A. Niemi, Associate Editor, John Wakabayashi, and two anonymous reviewers, whose critical comments and constructive evaluation have significantly improved the quality of the paper. The data used are available in the supporting information.

## References

- Aitchison, J. C., & Buckman, S. (2012). Accordion vs. quantum tectonics: Insights into continental growth processes from the Paleozoic of eastern Gondwana. *Gondwana Research*, 22(2), 674–680. <https://doi.org/10.1016/j.gr.2012.05.013>
- Aldanmaz, E., Yaliniz, M. K., Güctekin, A., & Göncüoğlu, M. C. (2008). Geochemical characteristics of mafic lavas from the Neotethyan ophiolites in western Turkey: Implications for heterogeneous source contribution during variable stages of ocean crust generation. *Geological Magazine*, 145(1), 37–54. <https://doi.org/10.1017/S0016756807003986>
- BGMROP (Bureau of Geology and Mineral Resources of Qinghai Province) (1964). Geological report of Xining (J-47-36) and Ledu (J-48-31) areas (in Chinese), 1:200000.
- BGMROP (Bureau of Geology and Mineral Resources of Qinghai Province) (1977). Geological report of Angsiduo (J-48-133-A) area (in Chinese), 1:50000.
- BGMROP (Bureau of Geology and Mineral Resources of Qinghai Province) (1991). *Regional geology of Qinghai Province* (in Chinese) (pp. 1–662). Beijing: Geological Publishing House.
- Boudier, F., & Nicolas, A. (1995). Nature of the Moho transition zone in the Oman ophiolite. *Journal of Petrology*, 36(3), 777–796. <https://doi.org/10.1093/petrology/36.3.777>
- Boutelier, D., & Chemenda, A. (2011). Physical modeling of arc-continent collision: A review of 2D, 3D, purely mechanical and thermo-mechanical experimental models. In D. Brown & P. D. Ryan (Eds.), *Arc-continent collision* (pp. 445–473). Berlin, Heidelberg: Springer-Verlag. [https://doi.org/10.1007/978-3-540-88558-0\\_16](https://doi.org/10.1007/978-3-540-88558-0_16)
- Brown, D., Ryan, P. D., Afonso, J. C., Boutelier, D., Burg, J. P., Byrne, T., et al. (2011). Arc-continent collision: The making of an orogeny. In D. Brown & P. D. Ryan (Eds.), *Arc-continent collision* (pp. 477–493). Berlin, Heidelberg: Springer-Verlag. [https://doi.org/10.1007/978-3-540-88558-0\\_17](https://doi.org/10.1007/978-3-540-88558-0_17)
- Buckman, S., & Aitchison, J. C. (2004). Tectonic evolution of Palaeozoic terranes in West Junggar Xinjiang, NW China. In J. Malpas, C. J. N. Fletcher, & J. C. Aitchison (Eds.), *Aspects of the tectonic evolution of China, Geological Society London Special Publications* (Vol. 226, pp. 101–129).
- Clift, P., & Vannucchi, P. (2004). Controls on tectonic accretion versus erosion in subduction zones: Implications for the origin and recycling of the continental crust. *Reviews of Geophysics*, 42, RG2001. <https://doi.org/10.1029/2003RG000127>
- Clift, P. D., Schouten, H., & Draut, A. E. (2003). A general model of arc-continent collision and subduction polarity reversal from Taiwan and the Irish Caledonides. In R. D. Larter & P. T. Leat (Eds.), *Intra-oceanic subduction systems: Tectonic and magmatic processes, Geological Society London Special Publications* (Vol. 219, pp. 81–98).
- Coleman, R. G. (1977). *Ophiolites* (pp. 1–110). New York: Springer. <https://doi.org/10.1007/978-3-642-66673-5>
- Dewey, J. F., & Bird, J. M. (1971). Origin and emplacement of the ophiolite suite: Appalachian ophiolites in Newfoundland. *Journal of Geophysical Research*, 76(14), 3179–3206. <https://doi.org/10.1029/JB076i014p03179>
- Dilek, Y., & Furnes, H. (2011). Ophiolite genesis and global tectonics: Geochemical and tectonic fingerprinting of ancient oceanic lithosphere. *Geological Society of America Bulletin*, 123(3–4), 387–411. <https://doi.org/10.1130/B30446.1>
- Dong, Y. P., He, D. F., Sun, S. S., Liu, X. M., Zhou, X. H., Zhang, F. F., et al. (2018). Subduction and accretionary tectonics of the East Kunlun orogen, western segment of the Central China Orogenic System. *Earth Science Reviews*. <https://doi.org/10.1016/j.earscirev.2017.12.006>
- Dong, Y. P., & Santosh, M. (2016). Tectonic architecture and multiple orogeny of the Qinling Orogenic Belt, Central China. *Gondwana Research*, 29(1), 1–40. <https://doi.org/10.1016/j.gr.2015.06.009>
- Elliott, T. (2003). Tracers of the slab. In J. Eiler & M. Hirschmann (Eds.), *Inside the subduction factory, Geophysical Monograph Series* (Vol. 138, pp. 23–46).
- Feng, Y. M., Cao, X. D., & Zhang, E. P. (2002). *Orogenic belt of the Western Qinling—Structure, process and dynamics* (in Chinese) (pp. 1–263). Xi'an: Xi'an Cartographic Publishing House.
- Fu, C. L., & Yan, Z. (2017). The composition, age and tectonic setting of Lajishan ophiolite mélange (in Chinese with English abstract). *Acta Geoscientia Sinica*, 38, 29–32.
- Fu, C. L., Yan, Z., Guo, X. Q., Niu, M. L., Cao, B., Wu, Q., et al. (2018). Assembly and dispersal history of continental blocks within the Altun-Qilian-North Qaidam mountain belt, NW China. *International Geology Review*, 1–24. <https://doi.org/10.1080/00206814.2018.1428831>
- Fu, C. L., Yan, Z., Guo, X. Q., Niu, M. L., Xia, W. J., Wang, Z. Q., & Li, J. L. (2014). Geochemistry and SHRIMP zircon U-Pb age of diorites in the Lajishankou ophiolitic mélange, South Qilian terrane (in Chinese with English abstract). *Acta Petrologica Sinica*, 30(6), 1695–1706.
- Gao, Y. L. (2000). Compiling the plate tectonic map on Qing-Tibet plateau (in Chinese with English abstract). *Qinghai Science and Technology*, 7(4), 14–18.

- Gribble, R. F., Stern, R. J., Bloomer, S., Studen, D., O'hearn, T., & Newman, S. (1996). MORB mantle and subduction components interact to generate basalts in the southern Mariana Trough back-arc basin. *Geochimica et Cosmochimica Acta*, *60*(12), 2153–2166. [https://doi.org/10.1016/0016-7037\(96\)00078-6](https://doi.org/10.1016/0016-7037(96)00078-6)
- Gribble, R. F., Stern, R. J., Newman, S., Bloomer, S. H., & O'hearn, T. (1998). Chemical and isotopic composition of lavas from the Northern Mariana trough: Implications for magmagenesis in back-arc basins. *Journal of Petrology*, *39*(1), 125–154. <https://doi.org/10.1093/ptrology/39.1.125>
- Guo, J. J., & Li, H. K. (1999). Angular unconformity between the Huashishan Group and Huangzhong Group in the Eastern Mid-Qilian Massif: Identification and implications (in Chinese with English abstract). *Progress in Precambrian Research*, *22*, 47–52.
- Guo, J. J., Zhang, G. W., Lu, S. N., Zhao, F. Q., Li, H. K., & Zheng, J. K. (1999). A discussion on the Proterozoic stratigraphy framework in the basement of eastern section of the Mid-Qilian Massif (in Chinese with English abstract). *Regional Geology of China*, *18*(4), 379–382.
- Guo, J. J., Zhao, F. Q., Li, H. K., Li, H. M., & Zuo, Y. C. (2000). New chronological evidence of the age of Huangyuan Group in the eastern segment of Mid-Qilian massif and its geological significance (in Chinese with English abstract). *Regional Geology of China*, *19*(1), 27–32.
- Hickey-Vargas, R., Savov, I. P., Bizimis, M., Ishii, T., & Fujioka, K. (2006). Origin of diverse geochemical signatures in igneous rocks from the West Philippine Basin: Implications for tectonic models. In D. M. Christie, C. R. Fisher, S.-M. Lee, & S. Givens (Eds.), *Back-arc spreading systems: Geological, biological, chemical, and physical interactions, Geophysical Monograph Series* (Vol. 166, pp. 287–303).
- Hou, Q. Y., Zhang, H. F., Zhang, B. R., Zhao, Z. D., & Zhu, Y. H. (2005). Characteristics and tectonic affinity of Lajishan Paleo-mantle in Qilian Orogenic Belt: A geochemical study of basalts (in Chinese with English abstract). *Earth Science*, *30*, 61–70.
- Hsü, K. J. (1968). Principles of mélanges and their bearing on the Franciscan-Knoxville paradox. *Geological Society of America Bulletin*, *79*(8), 1063–1071. [https://doi.org/10.1130/0016-7606\(1968\)79%5B1063:POMATB%5D2.0.CO;2](https://doi.org/10.1130/0016-7606(1968)79%5B1063:POMATB%5D2.0.CO;2)
- Huang, H., Niu, Y. L., Nowell, G., Zhao, Z. D., Yu, X. H., & Mo, X. X. (2015). The nature and history of the Qilian Block in the context of the development of the Greater Tibetan Plateau. *Gondwana Research*, *28*(1), 209–224. <https://doi.org/10.1016/j.gr.2014.02.010>
- Ishizuka, O., Taylor, R. N., Yuasa, M., Milton, J. A., Nesbitt, W., & Uto, K. (2007). Processes controlling along-arc isotopic variation of the southern Izu-Bonin arc. *Geochemistry, Geophysics, Geosystems*, *8*, Q06008. <https://doi.org/10.1029/2006GC001475>
- Ishizuka, O., Yuasa, M., Tamura, Y., Shukuno, H., Stern, R. J., Naka, J., et al. (2010). Migrating shoshonitic magmatism tracks Izu-Bonin-Mariana intra-oceanic arc rift propagation. *Earth and Planetary Science Letters*, *294*(1–2), 111–122. <https://doi.org/10.1016/j.epsl.2010.03.016>
- Ishizuka, O., Yuasa, M., Taylor, R. N., & Sakamoto, I. (2009). Two contrasting magmatic types coexist after the cessation of back-arc spreading. *Chemical Geology*, *266*(3–4), 274–296. <https://doi.org/10.1016/j.chemgeo.2009.06.014>
- Jousselin, D., & Nicolas, A. (2000). The Moho transition zone in the Oman ophiolite-relation with wehrlites in the crust and dunites in the mantle. *Marine Geophysical Researches*, *21*(3/4), 229–241. <https://doi.org/10.1023/A:1026733019682>
- Jung, C., Jung, S., Hoffer, E., & Berndt, J. (2006). Petrogenesis of Tertiary mafic alkaline magmas in the Hoheifel, Germany. *Journal of Petrology*, *47*(8), 1637–1671. <https://doi.org/10.1093/ptrology/egl023>
- Li, C. F., Li, X. H., Li, Q. L., Guo, J. H., & Li, X. H. (2011). Directly determining  $^{143}\text{Nd}/^{144}\text{Nd}$  isotope ratios using thermal ionization mass spectrometry for geological samples without separation of Sm-Nd. *Journal of Analytical Atomic Spectrometry*, *26*(10), 2012–2022. <https://doi.org/10.1039/c0ja00081g>
- Liang, Q., Jing, H., & Gregoire, D. C. (2000). Determination of trace elements in granites by inductively coupled plasma mass spectrometry. *Talanta*, *51*(3), 507–513. [https://doi.org/10.1016/S0039-9140\(99\)00318-5](https://doi.org/10.1016/S0039-9140(99)00318-5)
- Lin, T. R., Peng, S. C., & Zhou, Z. Q. (2015). Cambrian agnostoid trilobites from the Nidanshan and Liudaogou Groups, Hualong, northeastern Qinghai, China (in Chinese with English abstract). *Acta Palaeontologica Sinica*, *54*(2), 184–206.
- Manikyamba, C., Ganguly, S., Santosh, M., Singh, M. R., & Saha, A. (2015). Arc-nascent back-arc signature in metabasalts from the Neoproterozoic Jonnagiri greenstone terrane, Eastern Dharwar Craton, India. *Geological Journal*, *50*(5), 651–669. <https://doi.org/10.1002/gj.2581>
- Miyashiro, A. (1974). Volcanic rock series in island arcs and active continental margins. *American Journal of Science*, *274*(4), 321–355. <https://doi.org/10.2475/ajs.274.4.321>
- Moore, E. (1970). Ultramafics and orogeny, with models of the US Cordillera and the Tethys. *Nature*, *228*(5274), 837–842. <https://doi.org/10.1038/228837a0>
- Morimoto, N. (1988). Nomenclature of pyroxenes. *Mineralogy and Petrology*, *39*(1), 55–76. <https://doi.org/10.1007/BF01226262>
- Nicolas, A. (1989). *Structures of ophiolites and dynamics of oceanic lithosphere* (pp. 1–367). Dordrecht: Kluwer Academic Publishers. <https://doi.org/10.1007/978-94-009-2374-4>
- Nisbet, E. G., & Pearce, J. A. (1977). Clinopyroxene composition in mafic lavas from different tectonic settings. *Contributions to Mineralogy and Petrology*, *63*(2), 149–160. <https://doi.org/10.1007/BF00398776>
- Nohda, S., Tatsumi, Y., Yamashita, S., & Fujii, T. (1992). Nd and Sr isotopic study of Leg 127 Basalts: Implications for the evolution of the Japan Sea backarc basin. In K. Tamaki, K. Suyehiro, J. Allan, & S. McWilliams (Eds.), *Proceedings of the ocean drilling program, scientific results, 127/128, Pt 2* (pp. 899–904). College Station, TX.
- Parkinson, I. J., Pearce, J. A., Thirlwall, M. F., Johnson, K. T. M., & Ingram, G. (1992). Trace element geochemistry of peridotites from the Izu-Bonin-Mariana forearc, leg 125. In P. Fryer, J. A. Pearce, & L. B. Stokking (Eds.), *Proceedings of the ocean drilling program, scientific results, Vol. 125* (pp. 487–506). College Station, TX. <https://doi.org/10.2973/odp.proc.sr.125.183.1992>
- Pearce, J. A. (1982). Trace element characteristics of lavas from destructive plate boundaries. In R. S. Thorpe (Ed.), *Andesites: Orogenic andesites and related rocks* (pp. 525–548). Chichester: John Wiley and Sons.
- Pearce, J. A. (2008). Geochemical fingerprinting of oceanic basalts with applications to ophiolite classification and the search for Archean oceanic crust. *Lithos*, *100*(1–4), 14–48. <https://doi.org/10.1016/j.lithos.2007.06.016>
- Pearce, J. A. (2014). Immobility elements fingerprinting of ophiolites. *Elements*, *10*(2), 101–108. <https://doi.org/10.2113/gselements.10.2.101>
- Pearce, J. A., & Cann, J. R. (1973). Tectonic setting of basic volcanic rocks determined using trace element analyses. *Earth and Planetary Science Letters*, *19*(2), 290–300. [https://doi.org/10.1016/0012-821X\(73\)90129-5](https://doi.org/10.1016/0012-821X(73)90129-5)
- Pearce, J. A., & Peate, D. W. (1995). Tectonic implications of the composition of volcanic arc magmas. *Annual Review of Earth and Planetary Sciences*, *23*(1), 251–285. <https://doi.org/10.1146/annurev.ea.23.050195.001343>
- Pearce, J. A., Stern, R. J., Bloomer, S. H., & Fryer, P. (2005). Geochemical mapping of the Mariana arc-basin system: Implications for the nature and distribution of subduction components. *Geochemistry, Geophysics, Geosystems*, *6*, Q07006. <https://doi.org/10.1029/2004GC000895>
- Qiu, J. X., Zeng, G. C., Wang, S. Y., & Zhu, Y. H. (1997). *Early Paleozoic marine volcanic rocks and mineralization in Laji Mountains* (in Chinese with English abstract) (pp. 1–118). China University of Geosciences Press, Wuhan.



- Sengör, A. M. C., Natal'in, B. A., & Burtman, V. S. (1993). Evolution of the Altaid tectonic collage and Palaeozoic crustal growth in Eurasia. *Nature*, 364(6435), 299–307. <https://doi.org/10.1038/364299a0>
- Servais, J. W. (1982). Ti-V plots and the petrogenesis of modern and ophiolitic lavas. *Earth and Planetary Science Letters*, 59(1), 101–118. [https://doi.org/10.1016/0012-821X\(82\)90120-0](https://doi.org/10.1016/0012-821X(82)90120-0)
- Servais, J. W. (1990). Island arc and ocean crust ophiolites: Contrasts in the petrology, geochemistry and tectonic style of ophiolite assemblages in the California Coast Ranges. In J. Malpas, E. Moores, A. Panayiotou, & C. Xenophontos (Eds.), *Ophiolites oceanic crustal analogues: Proceedings of the symposium "Troodos 1987"* (pp. 507–520). Nicosia: The Geological Survey Department Ministry of Agriculture and Natural Resources.
- Smith, A. D., & Yang, H. Y. (2006). The neodymium isotopic and geochemical composition of serpentinites from ophiolitic assemblages in the Qilian fold belt, northwest China. *Journal of Asian Earth Sciences*, 28(2-3), 119–132. <https://doi.org/10.1016/j.jseae.2005.09.013>
- Song, S. G., Niu, Y. L., Li, S., Zhang, C., & Zhang, L. F. (2014). Continental orogenesis from ocean subduction, continent collision/subduction, to orogen collapse, and orogen recycling: The example of the North Qaidam UHPM belt, NW China. *Earth Science Reviews*, 129, 59–84. <https://doi.org/10.1016/j.earscirev.2013.11.010>
- Stern, R. J., Fough, M. J., & Klempner, S. L. (2003). An overview of the Izu-Bonin-Mariana subduction factory. In J. Eiler & M. Hirschmann (Eds.), *Inside the subduction factory, Geophysical Monograph Series* (Vol. 138, pp. 175–222).
- Sun, S. S., & McDonough, W. (1989). Chemical and isotopic systematics of oceanic basalts: Implications for mantle composition and processes. In A. D. Saunders & M. J. Norry (Eds.), *Magmatism in the ocean basins, Geological Society London Special Publications* (Vol. 42, pp. 313–345). <https://doi.org/10.1144/GSL.SP.1989.042.01.19>
- Taylor, R. N., & Nesbitt, R. W. (1998). Isotopic characteristics of subduction fluids in an intra-oceanic setting, Izu-Bonin Arc, Japan. *Earth and Planetary Science Letters*, 164(1-2), 79–98. [https://doi.org/10.1016/S0012-821X\(98\)00182-4](https://doi.org/10.1016/S0012-821X(98)00182-4)
- van Staal, C. R., & Barr, S. M. (2012). Lithospheric architecture and tectonic evolution of the Canadian Appalachians and associated Atlantic margin. In J. A. Percival, F. A. Cool, & R. M. Clowes (Eds.), *Tectonic styles in Canada: The lithoprobe perspective, Geological Association of Canada Special Paper* (Vol. 49, pp. 41–95).
- Wakabayashi, J. (2015). Anatomy of a subduction complex: Architecture of the Franciscan Complex, California, at multiple length and time scales. *International Geology Review*, 57(5-8), 669–746. <https://doi.org/10.1080/00206814.2014.998728>
- Wakabayashi, J. (2017a). Serpentinities and serpentinites: Variety of origins and emplacement mechanisms of serpentinite bodies in the California Cordillera. *Island Arc*, 26(5). <https://doi.org/10.1111/iar.12205>
- Wakabayashi, J. (2017b). Sedimentary serpentinite and chaotic units of the lower Great Valley Group forearc basin deposits, California: Updates on distribution and characteristics. *International Geology Review*, 59(5–6), 599–620.
- Wakabayashi, J. (2017c). Structural context and variation of ocean plate stratigraphy, Franciscan Complex, California: Insight into mélangé origins and subduction-accretion processes. *Progress in Earth and Planetary Science*, 4(1), 18. <https://doi.org/10.1186/s40645-017-0132-y>
- Wan, Y. S., Xu, Z. Q., Yang, J. S., & Zhang, J. X. (2003). The Precambrian high-grade basement of the Qilian terrane and neighboring areas: Its ages and compositions (in Chinese with English abstract). *Acta Geoscientia Sinica*, 24, 319–324.
- Wang, C., Li, R. S., Smithies, R. H., Li, M., Peng, Y., Chen, F. N., & He, S. P. (2017). Early Paleozoic felsic magmatic evolution of the western central Qilian belt, Northwestern China, and constraints on convergent margin processes. *Gondwana Research*, 41, 301–324. <https://doi.org/10.1016/j.gr.2015.12.009>
- Wang, E., Zhang, Q., & Burchfiel, C. B. (2000). The Lajishan fault belt in Qinghai province: A multi-staged uplifting structural window (in Chinese with English abstract). *Scientia Geologica Sinica*, 35, 493–500.
- Wang, Z. Q., Yan, Q. R., Yan, Z., Wang, T., Jiang, C. F., Gao, L. D., et al. (2009). New division of the main tectonic units of the Qinling Orogenic belt, Central China (in Chinese with English abstract). *Acta Geologica Sinica*, 83(11), 1527–1546.
- Weaver, B. L. (1991). Trace element evidence of the origin of ocean-island basalts. *Geology*, 19(2), 123–126. [https://doi.org/10.1130/0091-7613\(1991\)019%3C0123:TEFTO%3E2.3.CO;2](https://doi.org/10.1130/0091-7613(1991)019%3C0123:TEFTO%3E2.3.CO;2)
- Williams, I. S. (1998). U-Th-Pb geochronology by ion microprobe. *Reviews in Economic Geology*, 7, 1–35.
- Woodhead, J. D., Eggins, S. M., & Gamble, J. A. (1993). High field strength and transition element systematics in island arc and back-arc basin basalts: Evidence for multi-phase melt extraction and a depleted mantle wedge. *Earth and Planetary Science Letters*, 114(4), 491–504. [https://doi.org/10.1016/0012-821X\(93\)90078-N](https://doi.org/10.1016/0012-821X(93)90078-N)
- Xia, L. Q., Li, X. M., Yu, J. Y., & Wang, G. Q. (2016). Mid-late Neoproterozoic to early Paleozoic volcanism and tectonic evolution of the Qilianshan, NW China. *GeoResJ*, 9–12, 1–41.
- Xiao, W. J., Windley, B. F., Chen, H. L., Zhang, G. C., & Li, J. L. (2002). Carboniferous-Triassic subduction and accretion in the western Kunlun, China: Implications for the collisional and accretionary tectonics of the northern Tibetan Plateau. *Geology*, 30(4), 295–298. [https://doi.org/10.1130/0091-7613\(2002\)030%3C0295:CTSAAL%3E2.0.CO;2](https://doi.org/10.1130/0091-7613(2002)030%3C0295:CTSAAL%3E2.0.CO;2)
- Xiao, W. J., Windley, B. F., Liu, D. Y., Jian, P., Liu, C. Z., Yuan, C., & Sun, M. (2005). Accretionary tectonics of the Western Kunlun Orogen, China: A Paleozoic-Early Mesozoic, long-lived active continental margin with implications for the growth of southern Eurasia. *Journal of Geology*, 113(6), 687–705. <https://doi.org/10.1086/449326>
- Xiao, W. J., Windley, B. F., Sun, S., Li, J. L., Huang, B. C., Han, C. M., et al. (2015). A tale of amalgamation of three Permo-Triassic collage systems in Central Asia: Oroclines, sutures, and terminal accretion. *Annual Review of Earth and Planetary Sciences*, 43(1), 477–507. <https://doi.org/10.1146/annurev-earth-060614-105254>
- Xiao, W. J., Windley, B. F., Yong, Y., Yan, Z., Yuan, C., Liu, C. Z., & Li, J. L. (2009). Early Paleozoic to Devonian multiple-accretionary model for the Qilian Shan, NW China. *Journal of Asian Earth Sciences*, 35(3-4), 323–333. <https://doi.org/10.1016/j.jseae.2008.10.001>
- Yamamoto, S., Senshu, H., Rino, S., Omori, S., & Maruyama, S. (2009). Granite subduction: Arc subduction, tectonic erosion and sediment subduction. *Gondwana Research*, 15(3–4), 443–453. <https://doi.org/10.1016/j.gr.2008.12.009>
- Yan, Z., Aitchison, J., Fu, C. L., Guo, X. Q., Niu, M. L., Xiao, W. J., & Li, J. L. (2015). Hualong Complex, South Qilian terrane: U-Pb and Lu-Hf constraints on Neoproterozoic micro-continental fragments accreted to the northern Proto-Tethyan margin. *Precambrian Research*, 216, 65–82.
- Yan, Z., Xiao, W. J., Windley, B. F., Wang, Z. Q., & Li, J. L. (2010). Silurian clastic sediments in the North Qilian Shan, NW China: Chemical and isotopic constraints on their forearc provenance with implications for the Paleozoic evolution of the Tibetan Plateau. *Sedimentary Geology*, 231(3-4), 98–114. <https://doi.org/10.1016/j.sedgeo.2010.09.001>
- Yang, H., Zhang, H. F., Luo, B. J., Gao, Z., Guo, L., & Xu, W. C. (2016). Generation of peraluminous granitic magma in a post-collisional setting: A case study from the eastern Qilian orogen, NE Tibetan Plateau. *Gondwana Research*, 36, 15–32.
- Yu, M., Feng, C. Y., Santosh, M., Mao, J. W., Zhu, Y. F., Zhao, Y. M., et al. (2017). The Qiman Tagh Orogen as a window to the crustal evolution in northern Qinghai-Tibet Plateau. *Earth Science Reviews*, 167, 103–123.

- Zagorevski, A., & van Staal, C. R. (2011). The record of Ordovician Arc-Arc and Arc-Continent collisions in the Canadian Appalachians during the closure of Iapetus. In D. Brown & P. D. Ryan (Eds.), *Arc-continent collision* (pp. 445–473). Berlin, Heidelberg: Springer-Verlag. [https://doi.org/10.1007/978-3-540-88558-0\\_12](https://doi.org/10.1007/978-3-540-88558-0_12)
- Zhang, J. X., Yu, S. Y., & Mattinson, C. G. (2017). Early Paleozoic polyphase metamorphism in northern Tibet, China. *Gondwana Research*, *41*, 267–289. <https://doi.org/10.1016/j.gr.2015.11.009>
- Zhang, Y., Song, S., Yang, L., Su, L., Niu, Y., Allen, M. B., & Xu, X. (2017). Basalts and picrites from a plume-type ophiolite in the south Qilian Accretionary Belt, Qilian Orogen: Accretion of a Cambrian oceanic plateau? *Lithos*, *278-281*, 97–110. <https://doi.org/10.1016/j.lithos.2017.01.027>